JAN. - APR. 2022 ● Volume XXIII Number

# THE ASEAN JOURNAL OF RADIOLOGY

## Highlight

- Original Article
- Pictorial Essay
- ASEAN Movement in Radiology

Official Journal of

Radiological Society of Thailand

The Royal College of Radiologists of Thailand,

ASEAN Association of Radiology, and

Foundation for Orphan and Rare Lung Disease

ASEAN
JOURNAL OF RADIOLOGY

ISSN 2672-9393

# The ASEAN
## Journal of Radiology

# CONTENTS

THE ASEAN JOURNAL OF RADIOLOGY
ISSN 2672-9393

From The Editor

# The first hybrid annual congress of the Royal College of Radiologists of Thailand and the Radiological Society of Thailand: How we live with COVID-19

Received 20 April 2022 ; accepted 20 April 2022
doi:10.46475/aseanjr.v23i1.172

Thailand dropped its quarantine requirements for fully vaccinated international visitors in November 2021 to boost its battered economy which is heavily reliant on tourism. However, along with the renewal of tourism in Thailand, new COVID-19 infections have also begun to accelerate throughout the country. The rate of COVID-19 infection in Thailand rose from around 8, 000 new cases a day in the final week of January to more than 23, 000 new cases a day in the final week of February, surpassing the record set on 13 August 2021. At the beginning of this year, more than 90% of COVID-19 infected patientssuffered from Omicron, while the rest were infected with Delta until April when Omicron was expected to be 100% of the cause of the infection, according to the data from the Department of Medical Sciences. Even though the rate of infection was higher than in 2021, the severe cases and deaths were tremendously lower and did not cause shortage in care provision in the hospitals. This has brought us a promising sign that COVID-19 will become an endemic within this year. Aligning with this possibility, from 1 March 2022 onwards, the Ministry of Public Health launched the out-patient treatment system for COVID-19 infected people who were previously healthy and whose symptoms were mild. If things go as planned,

COVID-19 will be classified as an endemic disease by 1 July 2022. Whether or not COVID-19 will be comparable to the flu, death rates from these 2 viruses need to be compared. Globally, according to the World Health Organization [1], the flu-related deaths which vary from 290, 000 to 650, 000 cases per year seem to be tremendously lower than those caused by COVID-19. Thailand's National Communicable Disease Committee agreed on 13 criteria which must be met before COVID-19 can be categorised as an endemic disease in Thailand; for instances, new COVID-19 infections must not exceed 10,000 a day, the mortality rate must be less than 0.1% of the infection rate, the hospitalisation must stay lower than 10% of the infection rate and higher than 80% of those at high risk of developing serious symptoms must have received at least two doses of vaccine and the general population must have developed sufficient immunity. On 1 April 2022, land border checkpoints between Malaysia and Thailand reopened after being closed for more than 2 years due to the pandemic and the number of arrivals at Suvarnabhumi airport was nearly double to 11,000-12,000 passengers per day since the cancellation of the pre-arrival RT-PCR test requirements, but still far from 200,000 passengers per day in 2019, before the pandemic. During the Songkran (water splashing) Festival, taking place on 13-15 April, the longest holiday and most dynamic event in Thailand in which workers return to their hometowns, the celebration was allowed under the condition of strictly adherence to VUCA which stands for Vaccine (V), Universal precaution (U), COVID-free setting (C), and Antigen-test kit (A). Because it has been predicted that there would be a spike in cases and death rates within 1-2 weeks after the Songkran Festival, many provinces are preparing for this worst case scenario as well as trying to meet those 13 criteria afterwards.

Tuberculosis (TB)) is one of the 5 most common respiratory diseases (after pneumonia, asthma, chronic obstructive pulmonary disease, and lung cancer) [2] and has always been one of the most fatal infectious diseases of the world and in ASEAN countries since the ancient time. This year (2022) is the right time to move the End TB project which is the national policy to meet sustainable development goals (SDGs) that should have initiated since 2021 but was delayed by the COVID-19 pandemic. To cope with these 2 fatal diseases which affect human health by destroying lungs, a chest radiograph was chosen for screening

for tuberculosis and assessing the lung condition in COVID-19 infected people. To avoid overcrowding in the hospitals, mobile units into the communities to perform chest radiographs and provide tests for diagnosis are the adopted and promoted in all community hospitals.

*Mobile units from both public and private sections performing chest radiographs to screen for tuberculosis and assess the severity of COVID-19 infection in communities.*

Given the improved pandemic situation, the Royal College of Radiologists of Thailand (RCRT) and the Radiological Society of Thailand (RST) held their first hybrid but 58th annual congress during 23-25 March 2022 at Icon Siam, the megamall on the east bank of the Chao Phraya river, Bangkok, under the government's VUCA policy. The JF Advance Med Company who funded the RadioVolunteer Project [3] hosted volunteers in its thank you dinner party cruise along the Chao Phraya River in the evening of 22 March. In addition to an exhibition of novel technologies, a presentation of upcoming knowledge and research, and social functions during the 3 days of the congress, two sessions of knowledge sharing on tuberculosis were arranged under collaborations between the Asian Oceanian School of Radiology (AOSOR), RCRT, RST, and FUJIFILM (Thailand) company to support the government's End Tuberculosis policy.

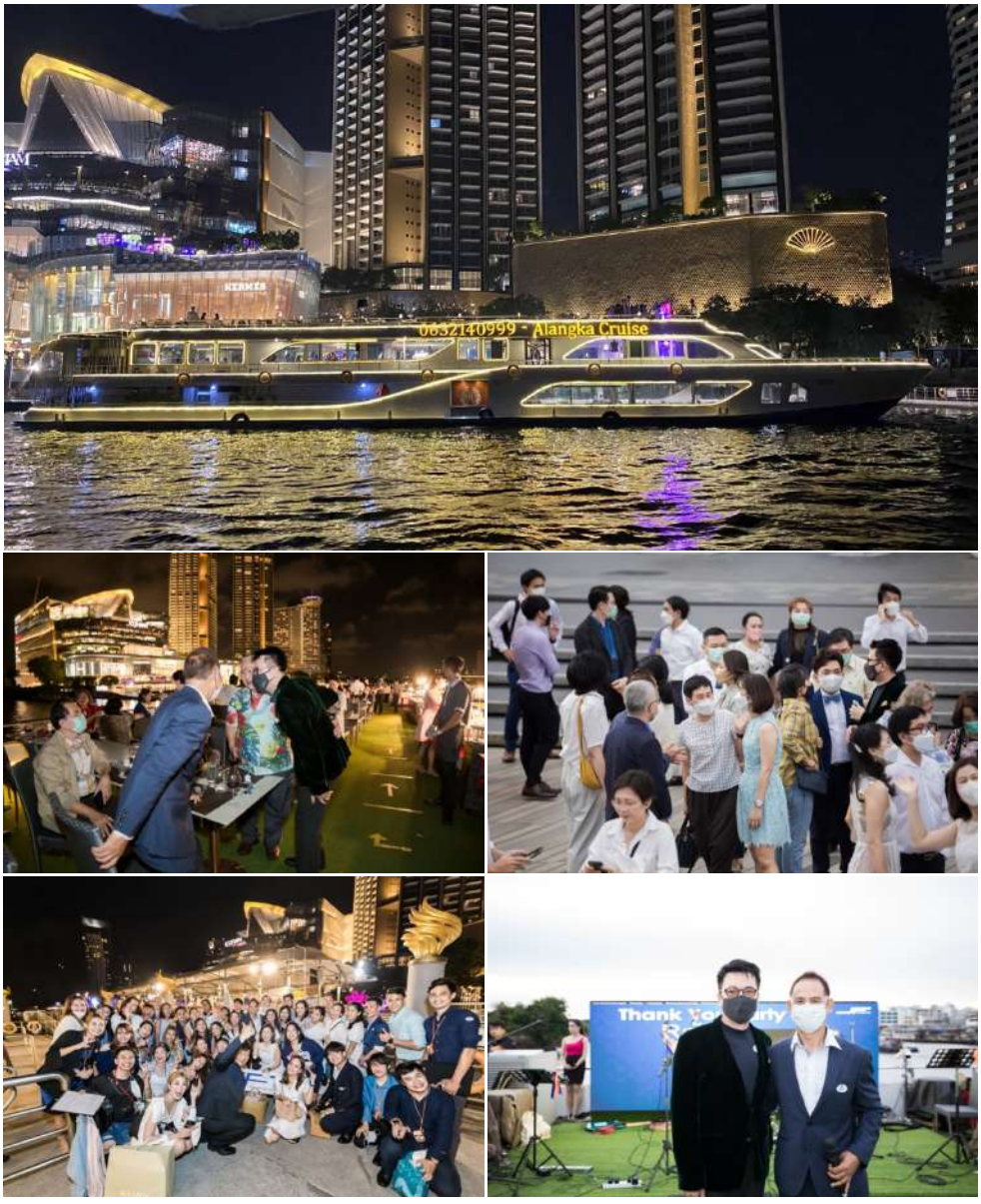


*The atmosphere in the pre-congress evening of 22 March 2022. Clockwise from top: Alangka Cruise, on which the thank you dinner party to volunteer radiologists took place, in front of Icon Siam; editor among volunteer radiologists awaiting on board; editor with Mr. Kajohn Uamsiri, managing director of JF Advance Med Company; editor and Mr. Uamsiri with Mr.Sala Ubolchai, President of Thai Society of Radiological Technologists, and Associated Professor Manus Mongkolsuk, Dean of Faculty of Radiological Technology, Rangsit University; Mr. Adisorn Taprig, general manager of the JF Advance Med Company, among company staff.*


*The first day of 58th RCRT-RST annual congress. Clockwise from top left: Editor as the RCRT President and Chair of the congress with the former President (Associate Professor Permyos Kosolphan), RCRT-RST board of directors, and lecturers; Editor as the RCRT President with the former Presidents (Associate Professor Anchalee Churojana and Associate Professor Permyos Kosolphan), teachers, and recently graduated radiologists and follows; Editor with Dr.Tawika Keawchur and Assistant Professor Warawut Sukkasem, as congress committee, and organizers visiting the exhibition.*

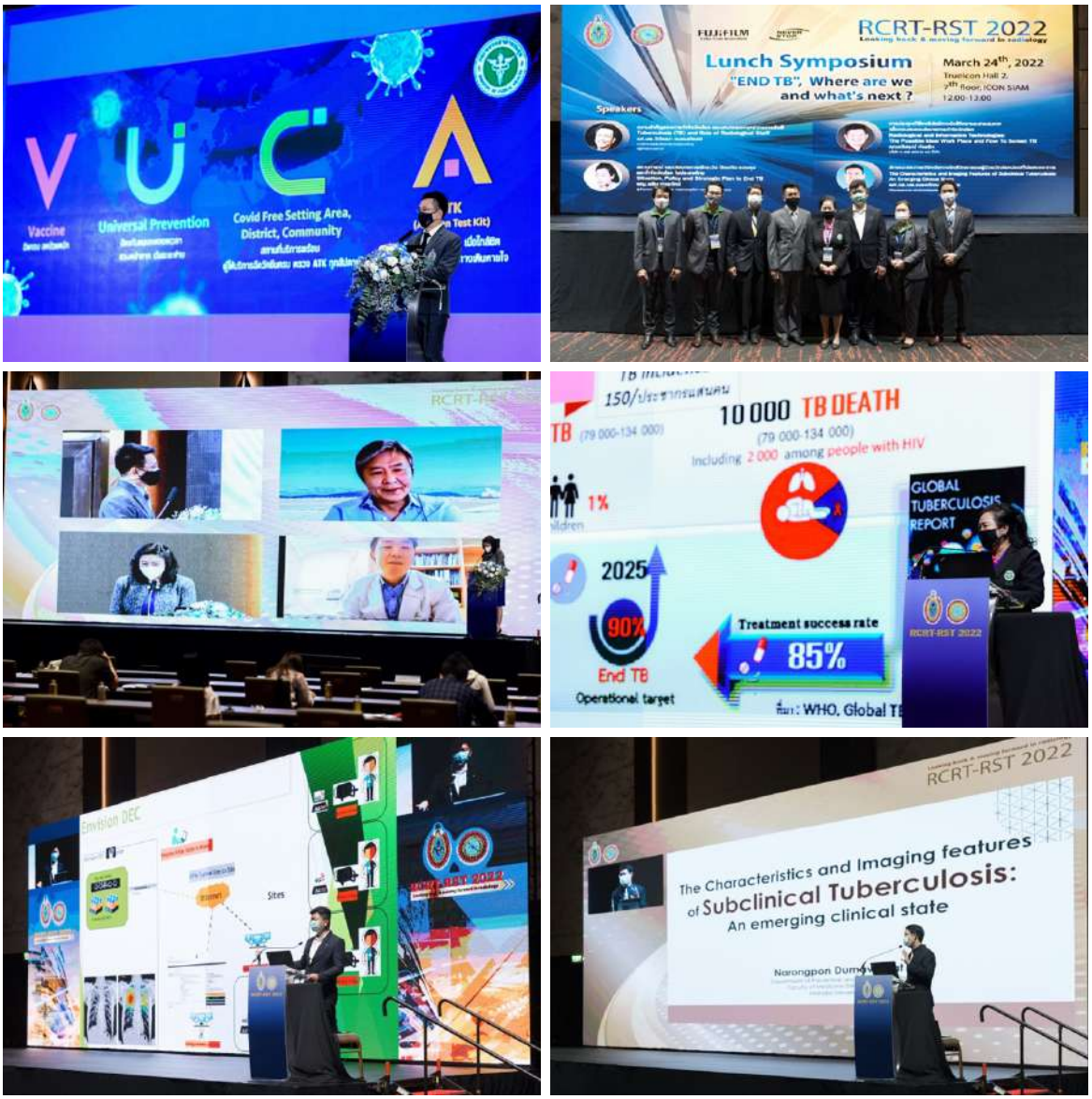


*Sessions on tuberculosis. Clockwise from top left: Editor as the RCRT President and Chair of the congress introduces the trendy VUCA concepts; Editor moderates a lunch symposium supported by FUJIFILM (Thailand) Company in which Dr. Phalin Kamolwat, Director of Bureau of Tuberculosis, presents the situation of tuberculosis in Thailand while Assistant Professor Narongpol Dumavibhat and Mr.Adisorn Taprig share points of views in their expertise; Associated Professor Nucharin Supakul moderates the RST-AOSOR conjoint session in which Dr. Ujita Masuo, Professor Soon Ho Yoon, and Associate Professor Li Fan share experiences and situations in their countries.*

THE ASEAN JOURNAL OF RADIOLOGY
ISSN 2672-9393

Thailand is one of the countries with the highest road traffic deaths. From 2020 to 2021, there were 34,788 road fatalities. With the rate of more than 35 per 100, 000 population means that there are more than 60 people a day or 2 people an hour killed by traffic accidents which is higher than the death rate from COVID-19. More than 95% of the deaths belonged motorcycle users and more than 60% occurred during nighttime [4]. Songkran Festival is so notorious for its 7 dangerous days in which people were more vulnerable to experiencing road accidents. At the time of writing, there were 1,917 traffic accidents, 1,869 injured people and 278 dead victims during the government's seven-day road safety campaign, five percent down from the figures reported annually in the past three years on average.

*Wiwatana Tanomkiat, M.D.*
Editor,
The ASEAN Journal of Radiology
**Email:** aseanjournalradiology@gmail.com

## References

1. World Health Organization [Internet]. Geneva: WHO; © 2022 [cited 2022 Apr 20]. WHO launches new global influenza strategy; [about 5 screens]. Available from: https://www.who.int/news/item/11-03-2019-who-launches-new-global-influenza-strategy

2. GBD Chronic Respiratory Disease Collaborators. Prevalence and attributable health burden of chronic respiratory diseases, 1990–2017: a systematic analysis for the Global Burden of Disease Study 2017. Lancet Respir Med 2020; 8:585–96. doi: 10.1016/S2213-2600(20)30105-3.
3. Tanomkiat W, Taprig A, Piyavisetpat N. RadioVolunteer, a novel combination of social, management and technological innovations by the Royal College of Radiologists of Thailand in response to the COVID-19 pandemic. ASEAN J Radiol [Internet]. 2021 [cited 2022 Apr 20]; 22(2):57-66. Available from: https://www.asean-journal-radiology.org/index.php/ajr/article/view/146/99

4. IPPD Institute of Public Policy and Development [Internet]. Bangkok: IPPD; © 2020 [cited 2022 Apr 20]. โควิดทำให้คิดใหม่ ทางเลือกของมาตรการลดอุบัติเหตุทางถนน; [about 14 screens]. Available from: ippd.or.th/roadsafety/. Thai.

Original Article

# Correlation between prediabetes, coronary artery calcification and cardiovascular risk factors: A 5-year retrospective case study

*Thunnawat Wattanaseth, M.D., Ph.D., ABAARM*[(1)]
*Mart Maiprasert , M.D., ABAARM* [(2)]
*Pattana Teng-Umnuay, M.D., Ph.D.*[(2)]
*Pansak Sugkraroek, M.D.*[(2)]
*Phawit Norchai , M.D., Ph.D., ABAARM*[(2)]
From [(1)] Medical Imaging Center, Kasemrad International Hospital, Nonthaburi, Thailand.
[(2)] Department of Anti-Aging and Regenerative Medicine, College of Integrative Medicine (CIM), Dhurakij Pundit University, Bangkok, Thailand.
Address correspondence to T.W. (e-mail: Thunnawatw@gmail.com)

Received 15 June 2021; revised 21 March 2022; accepted 28 March 2022
doi:10.46475/aseanjr.v23i1.136

## Abstract

**Objective:** To evaluate the correlation between prediabetes, Hemoglobin A1c (HbA1c) 5.7 to 6.4%, cardiovascular risks (determined by Framingham Risk Score: FRS) and the coronary artery calcium score (CACS), by the retrospective analysis of 5 year data documents on PACS, Jan 2015 to Dec 2020.

**Materials and Methods:** There were 1,639 eligible cases, reviewed by certified radiologists via Picture Archiving and Communication System (PACS), with an asymptomatic condition in the check-up center, divided into two groups: - (1) the prediabetes group, with 756 cases and (2) the non-diabetes group, with 883 cases. The results of vital signs, BMI, CACS, blood test, HbA1c, fasting blood sugar (FBS), lipid profiles, and serum uric acid of all eligible cases were reviewed.

THE ASEAN JOURNAL OF RADIOLOGY
ISSN 2672-9393

Linear regression, t-test, chi-square, and Adjusted Odd ratio were used analyzed the significance and correlation between variables.

**Results:** (1) Most of the prediabetes participants (456 cases, 60.31%) had an intermediate risk of Framingham Risk Score (FRS). While most of the non-diabetes participants (665 cases, 75.31%) had a low risk of FRS., with a statistical difference (Chi-square, $P < 0.05$), (2) The prediabetes cases were significantly associated with coronary calcification at 2.38 times to the non-diabetic cases [Adjusted Odds Ratio = 2.38 [95% CI (1.98 – 14.98)]., (3) The intermediate cardiovascular risk (FRS) was associated with positive coronary artery calcification at 2.36 times to the low cardiovascular risk [Multivariate adjusted OR = 2.36 (95% CI (1.06 – 5.46)]., and (4) The high cardiovascular risk (FRS) was associated with positive coronary artery calcification at 8.64 times to the low cardiovascular risk [Multivariate adjusted OR = 8.64 (95% CI (2.65 – 18.58)]. Moreover, we found a significant higher serum uric acid in the prediabetes group than the non-diabetes group.

**Conclusion:** Subclinical prediabetes, among 47 to 62-year-old individuals, with an intermediate risk of FRS was significantly associated with positive coronary calcification (atherosclerosis). The combination of CACS screening with a safety low dose radiation protocol and FRS are of complementary together to evaluate the potential risk of Atherosclerotic Cardiovascular Disease (ASCVD). The benefits of combining CACS and FRS are used for decision making of the statin therapy, according to the ACC/AHA primary prevention guidelines (2019). Moreover, a high serum uric acid (UA) is a new challenging ASCVD risk factor in the present that we found it in prediabetes. The association of UA, cardiometabolic disease, and coronary atherosclerosis needs further studies.

**Keywords:** Prediabetes, Coronary Artery Calcium Score, Framingham Risk Score.

## Introduction

According to the American Diabetes Association [1], prediabetes is a metabolic stage between normal glucose homeostasis and diabetes, by HbA1c value of 5.7 – 6.4%. It can develop diabetes and atherosclerotic cardiovascular disease (ASCVD) in the future. The continuing increase in the prevalence of diabetes mellitus and prediabetes in the general population is predicted to result in a higher incidence of coronary artery disease (CAD), ischemic heart disease (IHD) and Atherosclerotic Cardiovascular Disease (ASCVD).

In 2019, the American Heart Association guideline [2] suggests that coronary artery calcium (CAC) testing may be considered in adults of 40 -75 years of age without diabetes mellitus and with the LDL-C level > 70 to 189 mg/dL at a 10-year atherosclerotic cardiovascular disease (ASCVD) risk of 7.5% to 20%.

In the present, subclinical prediabetes have been increasing in general population which has lifestyle dealing with high glycemic food, high sugar intake, fast foods, oxidative stress, inadequate exercise, and no available time for health checkup.

The benefit of combination of CACS screening with the safety low dose radiation protocol and FRS is an early detection of coronary atherosclerosis and evaluation of the potential risk of Atherosclerotic Cardiovascular Disease (ASCVD). This is an important state of the art for the statin therapy and lifestyle modification, according to the ACC/AHA primary prevention guidelines (2019).

## Research objective

The objective the study was to evaluate the correlation between prediabetes (HbA1c 5.7 to 6.4%), cardiovascular risks (determined by Framingham Risk Score: FRS) and coronary artery calcium (CAC), by a retrospective analysis of 5 year data documents, Jan 2015 to Dec 2020.

THE ASEAN JOURNAL OF RADIOLOGY
ISSN 2672-9393

## Materials and methods

### Study design, data collection and participants

The participants were asymptomatic cases of a check-up center who were identified by reviewed medical records in PACS (Picture Archive and Communication System) and HIS (Hospital Information System) of Kasemrad International Hospital, Thailand, during Jan 2015 to December 2020. All cases of CACS received scan by a 256-slice iCT scanner Philips with the standard protocol of CACS. All cases of CACS were interpreted by certified radiologists. This research was approved by the Human Research Ethics Review Board of Dhurakij Pundit University since March 24, 2021.

**Inclusion criteria** were cases of the check-up center with CACS, during January 2015 to December 2020, who had less HbA1c than 6.5% and less fasting blood sugar (FBS) than 126 mg/dL and had a blood test of lipid profiles and uric acid.

**Exclusion criteria** were known cases of ischemic heart disease, coronary balloon, coronary stent, diabetes mellitus, hypertension, autoimmune disease, gout, cancer, advanced renal disease (GFR < 40 ml/minutes), liver disease, statin therapy, antihypertensive therapy, steroid therapy, and received bisphosphonates.

**Participants** were classified into two groups: (1) non-diabetic group: HbA1c < 5.7% and FBS < 100 mg/dL and (2) prediabetes group: HbA1c 5.7 to 6.4% and FBS < 126 mg/dL

**The CT coronary calcium (CAC)** score was classified into four levels, as follows: level 1 CAC = 0 (extremely low risk), level 2 CAC is 1-10 (low risk), level 3 CAC is 11-100 (moderate risk), level 4 CAC is 101-400 (high risk), and level 5 CAC > 400 (extremely high risk for coronary artery disease).

**The percentage of Glycated hemoglobin (HbA1c)** was classified into four intervals: class interval 1: HbA1c ≤ 5.4%, class interval 2: 5.4% < HbA1c <5.7%, class interval 3:5.7% ≤ HbA1c < 5.9%, and class interval 4: 5.9% ≤ HbA1c ≤ 6.4%

**Framingham Risk Score (FRS)** was classified to three categories: category 1: FRS ≤ 10% (low risk of CVD), category 2: 10% < FRS ≤ 19% (Intermediate risk for CVD), and category 3: FRS ≥ 20% (High risk for CVD)

Statistics used were *t* test, Chi-square, Cramer's V, and the Logistic Regression Model.

The adjustment of confounding factors between groups was used by adjusting the Odd Ratio.

The difference of a 10-year mean age between the two groups in the study was adjusted by the weighted factor of FRS in each group.

## Results

There were 1,639 eligible cases, reviewed on PACS, divided into two groups: (1) the prediabetes group, with 756 cases and (2) the non-diabetes group, with 883 cases. The mean age of the prediabetes group, 54.84 ± 6.87 years, was older than the non-diabetes group, 44.82 ± 7.83 years. The BMI of the prediabetes group, with the average of 27.9 kg/m$^2$, was significantly higher than that of the non-diabetic group with the average of 21.6 kg/m$^2$, (P-value = 0.036). The total cholesterol and LDL of the prediabetes group, 199.50 ± 36.7mg/dL and 142 ± 14.8 mg/dL, were significantly higher than those of the non-diabetic group, 158.40 ± 34.9mg/dL and 98 ± 12.8mg/dL, P-value = 0.012 and 0.023, respectively, as seen in Table 1.

Most of the prediabetes participants (456 cases, 60.31%) had an intermediate cardiovascular risk score (Framingham Risk Score: FRS). While most of the non-diabetes participants (665 cases, 75.31%) had low risk of FRS., with statistical difference (Chi-square, P < 0.05), seen in Table 2.

Most of the CACS range in the prediabetes group was 11-100 (272 cases, 35.9%). Most of the CACS in the non-diabetes group was zero (743 cases, 84.1%).

THE ASEAN JOURNAL OF RADIOLOGY
ISSN 2672-9393

Overall, the highest range of CACS among the participants was zero (926 cases from 1,639cases, 56.49%), and then the CACS 11-100 (326 cases, 19.89%), seen in Table 3, Figure 1.

There was a significant relationship between the diabetic status (prediabetes and non-diabetes) and the presence of coronary artery calcification, with adjusted Odds Ratio of 2.38 [95% CI (1.98– 14.46)]. That means in cases of prediabetes, there was 2.38 times more to present with coronary artery calcification.

The intermediate cardiovascular risk (FRS) was associated with positive coronary artery calcification at 2.36 times to the low cardiovascular risk [Multivariate adjusted OR = 2.36 (95% CI (1.06 – 5.46)]. The high cardiovascular risk (FRS) was associated with positive coronary artery calcification at 8.64 times to the low cardiovascular risk [Multivariate adjusted OR = 8.64 (95% CI (2.65 – 18.58)], seen in Table 4.

**Table 1.** *Baseline characteristics of the study participants.*

| Demographic Characteristics | Prediabetes (n = 756) | Non-diabetes (n = 883) | P-value |
|---|---|---|---|
| Age, mean (SD) | 54.84 ± 6.87 | 44.82 ± 7.83 | 0.003* |
| Male (%) / Female (%) | 416 (55%) / 340 (45%) | 399 (46%) / 484 (54%) | 0.47 |
| HbA1c, mean (range) | 6.2 (5.7 – 6.4%) | 5.1 (4.8 - 5.6%) | < 0.001* |
| Fasting Blood Sugar (mg/dL), mean (range) | 112 (100 – 124) | 91 (86 - 99) | < .0001* |
| History of smoking, n (%) | 98 (13%) | 101 (12%) | 0.45 |
| Total Cholesterol (mg/dL), mean (SD) | 199.50 (36.7) | 158.40 (34.9) | 0.012* |
| HDL (mg/dL), mean (SD) | 48.3 (13.6) | 51.4 (10.2) | 0.15 |
| LDL (mg/dL), mean (SD) | 142 (14.8) | 98 (12.8) | 0.023* |
| Triglyceride (mg/dL), mean (SD) | 144 (28.8) | 136 (26.4) | 0.14 |
| Systolic Blood Pressure | 128 (8.6) | 118 (6.8) | 0.51 |
| (mmHg), mean (SD) | 128 (8.6) | 118 (6.8) | 0.51 |
| BMI ($Kg/m^2$), median (IQR) | 27.9 (7.3) | 21.6 (5.2) | 0.036* |
| Uric acid (mg/dL), mean (SD) | 5.28(1.38) | 3.82 (1.13) | <0.001* |

** P-value < 0.05*

**Table 2.** *Percentage of cardiovascular risk by Framingham Risk Score (FRS) in prediabetes and non-diabetes.*

| Framingham Risk Score (FRS) | Pre-diabetes n (%) | Non-diabetes n (%) | Total | P-value |
|---|---|---|---|---|
| Low Risk (< 10%) | 278 (36.77%) | 665 (75.31%) | **943** | 0.036* |
| Intermediate Risk (10-19%) | 456 (60.31%) | 211(23.59%) | **667** | 0.016* |
| High Risk (≥20%) | 22 (2.91%) | 7 (0.79%) | **29** | 0.057 |
| **Total** | **756** | **883** | **1,639** | |

** P-value < 0.05*

**Table 3.** *Percentage of CACS in prediabetes and non-diabetes.*

| CACS | Pre-diabetes Cases (n, %) | Non-diabetes Cases (n, %) | P-value |
|---|---|---|---|
| CACS = 0 | 183 (24.2%) | 743 (84.1%) | **0.016*** |
| CACS 1 -10 | 174 (23.0%) | 84 (9.5%) | **0.367** |
| CACS 11-100 | 272 (35.9%) | 54 (6.1%) | **0.013*** |
| CACS 101-400 | 118 (15.6%) | 2 (0.2%) | **0.002*** |
| CACS > 400 | 9 (1.2%) | 0 | **< 0.001*** |
| **Total** | **756** | **883** | **1,639** |

** P-value < 0.05*


**Figure 1.** *CT coronary artery calcium score (CACS) in a 64-year-old female, HbA1c 6.3% with moderate cardiovascular risk (FRS = 13%), CACS = 202.3.*

**Table 4.** *Logistic regression model of positive coronary artery calcification score (CACS > 0) of participants divided by Framingham Risk Score (FRS)*.*

| Participants with Framingham Risk Score (FRS) | No. of participants with positive CACS > 0 | Multivariate OR (95% CI) |
|---|---|---|
| **Prediabetes** | | |
| • Low Risk (< 10%) | 216 | 1.00 (reference) |
| • Intermediate Risk (10-19%) | 339 | 2.36 (1.06 – 5.46) |
| • High Risk (≥20%) | 18 | 8.64 (2.65 – 18.58) |
| **Non-diabetes** | | |
| • Low Risk (< 10%) | 16 | 1.00 (reference) |
| • Intermediate Risk (10-19%) | 121 | 7.86 (3.08-18.18) |
| • High Risk (≥20%) | 3 | 3.70 (1.59- 8.65) |
| **P for trend** | | **< 0.001** |

**Logistic regression model was used to estimate OR and 95% CI*
*Model: adjustment for BMI, LDL, triglyceride, and uric acid.*

THE ASEAN JOURNAL OF RADIOLOGY
ISSN 2672-9393

## Discussion

The significant results of the 5-year retrospective case study which analyzed the correlation between prediabetes, HbA1c 5.7 to 6.4%, cardiovascular risks determined by Framingham Risk Score (FRS) and coronary artery calcium score (CACS) represent performance and potential usage of CACS. CACS can explore coronary atherosclerosis in prediabetes with an intermediate risk of FRS. The combination of CACS and FRS is complementary to evaluate the potential risk of CVD. The benefits of results can be used for decision making of the statin therapy and lifestyle modification, according to the ACC/AHA primary prevention guidelines (2019). There are four issues during decision making, as follows:

**1. The Power of CACS Testing**

On March 5, 2022, there was a recent Asia Pacific symposium of SCCT (Society of Cardiovascular Computed Tomography) in Hong Kong [3]. The meeting reveals the power of coronary artery calcium (CAC) scanning in the situation of screening Atherosclerotic Cardiovascular Disease (ASCVD) and planning prevention, according to the ACC/AHA guideline on management of blood cholesterol (2018) [4]. The most important recent observation studies have been the findings that a CACS of zero indicates a low ASCVD risk for the subsequent 10 years.

Many studies found a significant positive association between CAC and inflammation of blood vessels, an inflammatory pathway of cytokines, C-reactive protein, aging, degenerative process, diabetes, prediabetes, metabolic syndrome, dyslipidemia, non-communicable diseases (NCDs), dyslipidemia, and a family history of premature coronary heart disease. In our study, the findings and results were consistent with well-known worldwide studies [5,6,7] as shown in the symposium. The CACS is the power of screening ASCVD in patients with low to intermediate CVD risks (by Framingham Risk Score) to prevent further morbidity of ASCVD.

**2. Is Uric Acid a CVD Risk Factor?**

Uric acid (UA) is a new challenging ASCVD risk factor in the present. The recent scientific studies [8-11] show association between uric acid and cardiovascular disease via the fructose (pentose) phosphate pathway. Consuming fructose-sweetened and beverages increases visceral fat, decreases insulin sensitivity, and promotes diabetes. An excessive level of fructose will increase the serum uric acid via the fructose (pentose) phosphate pathway. Uric acid (UA) is the final product of purine metabolism. It is a well-known risk factor for gout. Moreover, a high level of serum UA is also a biomarker for cardiovascular disease (CVD) morbidity and mortality [6].

**3. Radiation Dose of CAC Scanning**

The radiation dose exposure in CAC scanning is less than 1 mSV with care dose protocol for patients' safety as ALARA principle (As Low as Reasonably Achievable), named "i-care" software in Philips 256-slice CT scanner of our study, CARE (Combined Applications to Reduce Exposure) and SAFIRE (Sinogram Affirmed Iterative Reconstruction) in Siemen's scanner, and SURE-Exposure technology in Cannon scanner.

**4. Benefit of Combination CACS and FRS for Evaluation ASCVD**

FRS represents a prediction of CVD, while CACS represents evidence of coronary atherosclerosis. The combination of CACS and FRS evaluate ASCVD complements each other. According to the ACC/AHA primary prevention guidelines (2019), the statin therapy was recommended in two groups: (1) CACS 1-99 especially after the age of 55, and (2) CACS ≥ 100 and /or ≥ 75$^{th}$ percentile. This is an obvious benefit of CACS in the clinical practice guideline for decision making regarding the statin therapy.

THE ASEAN JOURNAL OF RADIOLOGY
ISSN 2672-9393

## Conclusion and suggestion

Subclinical prediabetes with an intermediate risk of FRS and the presence of coronary artery calcification (atherosclerosis) should be treated with a statin therapy and lifestyle modification according to the AHA guideline (2019). CACS screening in these patients benefit their lives in the long run. The role of preventive medicine and health promotion depend on the combination of CACS and FRS for screening. In fact, FRS represents a prediction of ASCVD, while CACS represents evidence of coronary atherosclerosis. The combination of CACS and FRS to evaluate ASCVD complements each other.

## References

1. American Diabetes Association. 2. Classification and Diagnosis of Diabetes. Diabetes Care. 2017 Jan;40(Suppl 1): S11-S24. doi: 10.2337/dc17-S005.

2. Arnett DK, Blumenthal RS, Albert MA, Buroker AB, Goldberger ZD, Hahn EJ, et al. 2019 ACC/AHA Guideline on the Primary Prevention of Cardiovascular Disease: a report of the American College of Cardiology/ American Heart Association Task Force on Clinical Practice Guidelines. Circulation 2019;140: e596-e646. doi: 10.1161/CIR.0000000000000678.

3. Society of Cardiovascular Computed Tomography. Asia Pacific Symposium of SCCT [Internet]. 2022. [cited 2022 Apr 1]. Available from https://scct.org/events/EventDetails.aspx?id=1604244&group=

4. American College of Cardiology (ACC) and American Heart Association (AHA). 2018 Guideline on the Management of Blood Cholesterol Guideline [Internet]. Washington, DC: ACC/AHA [updated June 2019, cited 2022 Mar 1]. Available from: https://www.acc.org/~/media/Non-Clinical/Files-PDFs-Excel-MS-Word-etc/Guidelines/2018/Guidelines-Made-Simple-Tool-2018-Cholesterol.pdf

5. Nasir K, Shaw LJ, Budoff MJ, Ridker PM, Peña JM. Coronary artery calcium scanning should be used for primary prevention: pros and cons. JACC Cardiovasc Imaging 2012;5:111-8. doi: 10.1016/j.jcmg.2011.11.007.

6. Budoff MJ, Young R, Lopez VA, Kronmal RA, Nasir K, Blumenthal RS, et al. Progression of coronary calcium and incident coronary heart disease events: MESA (Multi-Ethnic Study of Atherosclerosis). J Am Coll Cardiol 2013; 61:1231-9. doi: 10.1016/j.jacc.2012.12.035.

THE ASEAN JOURNAL OF RADIOLOGY
ISSN 2672-9393

7. Silverman MG, Blaha MJ, Krumholz HM, Budoff MJ, Blankstein R, Sibley CT, et al. Impact of coronary artery calcium on coronary heart disease events in individuals at the extremes of traditional risk factor burden: the Multi-Ethnic Study of Atherosclerosis. Eur Heart J 2014; 35:2232-41. doi: 10.1093/eurheartj/eht508.

8. Caliceti C, Calabria D, Roda A, Cicero AFG. Fructose intake, serum uric acid, and cardiometabolic disorders: a critical review. Nutrients 2017; 9:395. doi: 10.3390/nu9040395.

9. Borghi C. The role of uric acid in the development of cardiovascular disease. Curr Med Res Opin 2015;31 Suppl 2:1-2. doi: 10.1185/03007995.2015.1087985.

10. Higgins P, Dawson J, Lees KR, McArthur K, Quinn TJ, Walters MR. Xanthine oxidase inhibition for the treatment of cardiovascular disease: a systematic review and meta-analysis. Cardiovasc Ther 2012; 30:217-26. doi: 10.1111/j.1755-5922.2011.00277.x.

11. Stack AG, Hanley A, Casserly LF, Cronin CJ, Abdalla AA, Kiernan TJ, et al. Independent and conjoint associations of gout and hyperuricaemia with total and cardiovascular mortality. QJM 2013; 106:647-58. doi: 10.1093/qjmed/hct083.

Pictorial Essay

# Imaging of mucormycosis during the COVID-19 pandemic: A pictorial review

*Utsav Ganguly, M.B.B.S.*[(1)]
*Shalini Agarwal, M.D., D.N.B.* [(1)]
*Bhavna Arora, D.N.B.*[(1)]
*Aditya Bhargava, M.S.*[(2)]
*Virender Singh, M.D.S.*[(3)]
*Chandni Sharma, M.S.*[(2)]
From [(1)] Department of Radiodiagnosis,
[(2)] Department of ENT,
[(3)] Department of oral and maxillofacial surgery,
Pt B.D. Sharma PGIMS, Rohtak 124001 (Haryana), India.
Address correspondence to U.G. (e-mail: utsav.ganguly22@gmail.com)

Received 25 August 2021 ; revised 25 December 2021 ; accepted 28 January 2022
doi:10.46475/aseanjr.v23i1.150

## Abstract

During the second wave of the coronavirus disease 2019 (COVID-19) pandemic, there was a significant rise in cases of rhino-orbito-cerebral mucormycosis (ROCM), an invasive form of acute fungal rhinosinusitis with a propensity for rapid spread to the orbits and intracranial compartment.

Prompt diagnosis and subsequent intervention in the form of surgical debridement and administration of antifungals is the mainstay of management of ROCM. Radiology plays a key role in the diagnosis of the disease and in the assessment of the extent of spread. This article serves to elaborate on the significant

THE ASEAN JOURNAL OF RADIOLOGY
ISSN 2672-9393

computed tomography (CT) and magnetic resonance imaging (MRI) findings in patients with ROCM. It is based on imaging findings of 146 microbiologically/histopathologically proven cases that were presented to our institute for management during the second wave (April-June 2021).

While CT gives excellent details of bony anatomy, particularly of bony rarefaction, it has limitations in terms of assessment of soft tissue spread. MRI provides excellent soft tissue delineation and helps with the assessment of the involvement of orbit, particularly the orbital apex, as well as intracranial extension.

**Keywords:** Mucormycosis, COVID 19, Radiology.

## Introduction and pathogenesis

Mucormycosis is a form of zygomycosis, an invasive and rapidly progressive infection caused by fungi of class Zygomycetes and order Mucorales, the most common species being *Rhizopus oryzae*. The first case reported in the literature was in 1885 by Paultauf [1]. However, the first case of mucormycosis was possibly one described by Friedrich Küchenmeister in 1855 [2]. In 1968, Clark proposed the term "mucormycosis" for diseases caused by species of the order Mucorales [3].

Mucormycosis is characterized by extensive angioinvasion with resultant thrombi in blood vessels leading to local gangrene and eschar formation. This might explain the involvement of perisinus soft tissue without frank bony destruction [4].

## Rhino-orbito-cerebral mucormycosis (ROCM)

It originates in the paranasal sinuses following the inspiration of spores. Due to angioinvasion, it quickly spreads to the surrounding areas. Symptoms depend on the extent of spread at the time of presentation.
Honavar et al. [5] proposed a four-stage system to determine the anatomical extent and severity of ROCM. These are:
Stage 1: Disease limited to nasal mucosa
Stage 2: Extension into paranasal sinuses
Stage 3: Involvement of orbit
Stage 4: Involvement of CNS

The significant risk factors include diabetes mellitus especially uncontrolled cases, corticosteroid therapy, organ or bone marrow transplantation, neutropenia, trauma, and burns [4]. Diabetes mellitus is an independent risk factor for both severe COVID-19 as well as mucormycosis [6]. Roden et al. found that 33 percent of their 929 patients with ROCM had a history of diabetes [1].

## Role of imaging

Imaging determines the extent of spread and plays a crucial role in establishing a diagnosis. The extent of spread dictates the extent of debridement required.

CT is the first-line investigation as it is cheaper and quicker, especially for a high patient load or sick patients. It gives an excellent delineation of rarefaction and focal dehiscence of bone (Figure 1). Extra-sinus spread to the orbital apex and other structures can also be detected on CT. However, very early, subtle involvement might be missed (Figure 2 and 3). It also gives an idea about the normal anatomical variants of the paranasal sinuses, which is important in case of patients planned for Functional Endoscopic Sinus Surgery (FESS) (Figure 4) [7].

THE ASEAN JOURNAL OF RADIOLOGY
ISSN 2672-9393

Middlebrooks et al. performed multivariate analysis and devised a 7-variable model to assess sensitivity, specificity, and positive and negative predictive values for mucormycosis. The variables included periantral fat, bony dehiscence, orbital involvement, septal ulceration, pterygopalatine fossa, nasolacrimal duct, and lacrimal sac. The number of these sites that were involved dictated the sensitivity and specificity for mucormycosis [8].

MRI, on the other hand, provides excellent delineation of soft tissues, both of the intracranial compartment as well as the extracranial head and neck. It can pick up subtle involvement of crucial areas like the orbital apex and cavernous sinus, which may be missed out on a CT scan. MRI is warranted to take a closer look if CT shows abnormalities.

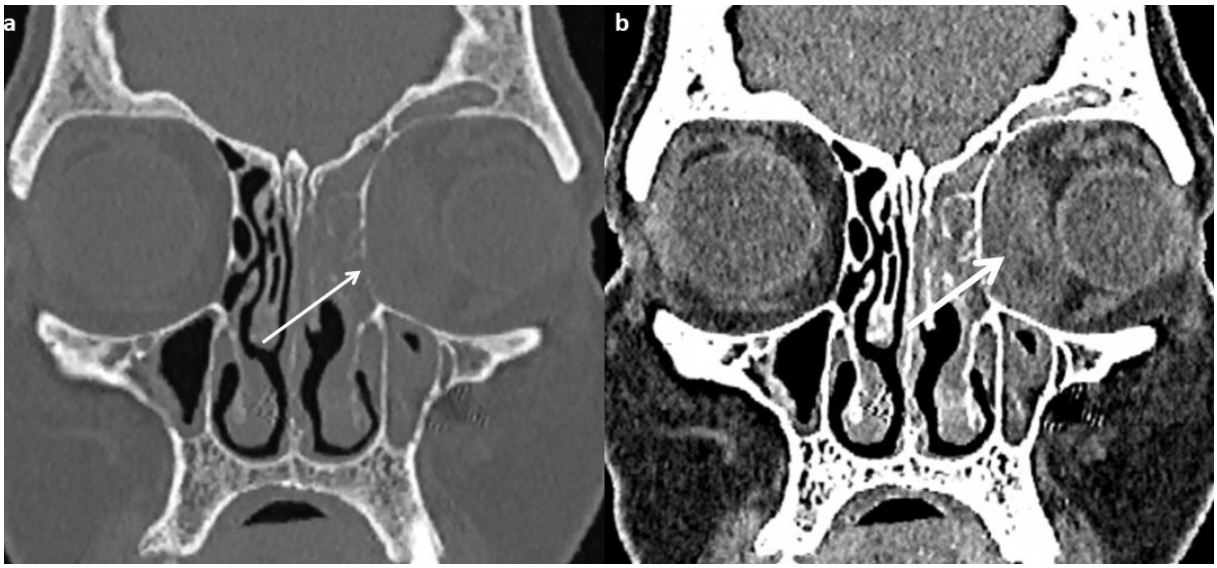


**Figure 1.** *Coronal reformatted CT in (a) bone and (b) soft tissue window reveals thinning of ethmoid air cells and lamina papyracea (thin arrow). There is a soft tissue lesion in the left ethmoid air cells as well as in the medial aspect of the left orbit with thickening of the medial rectus muscle and displacement of globe laterally (thick arrow).*

**Figure 2.** *Axial CT shows soft tissue material in the preantral (thin arrow) and the retroantral spaces (thick arrow) on the right side, with bulky muscles of mastication.*

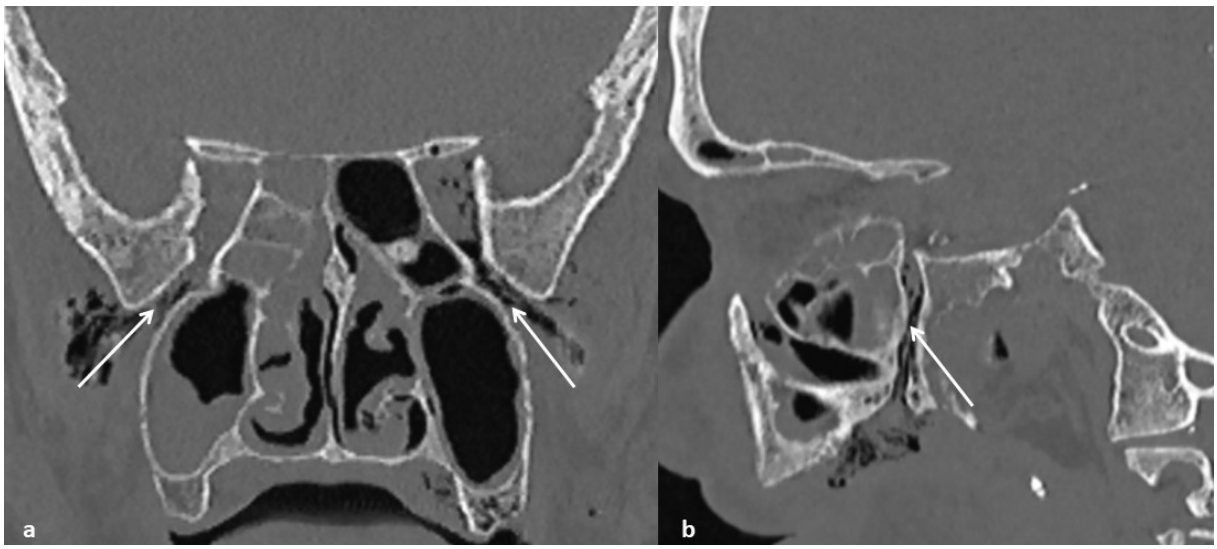


**Figure 3.** *(a) Coronal reformatted CT shows multiple air foci extending from pterygopalatine fossa to infratemporal fossa bilaterally (arrows). (b) Sagittal reformatted CT shows multiple air foci extending from pterygopalatine fossa to oral cavity via the palatine canal (arrow).*

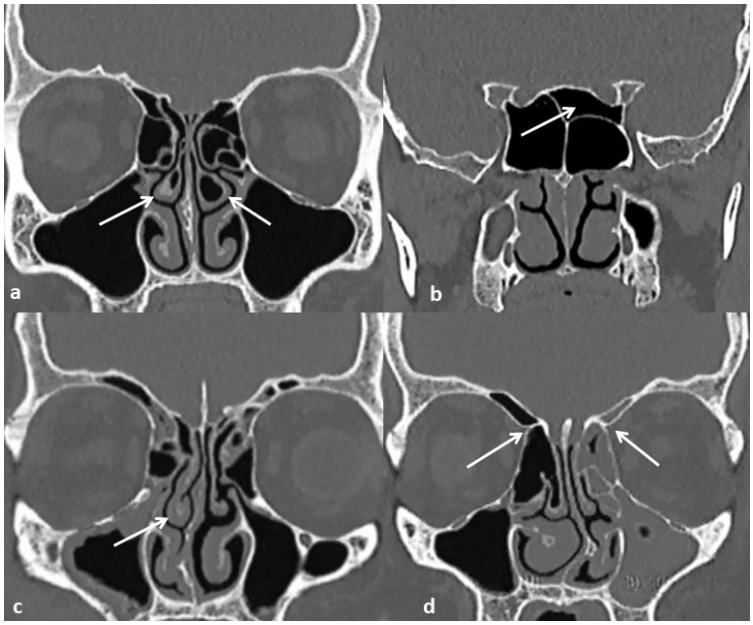


**Figure 4.** *Coronal reformatted CT showing some common anatomical variants of the paranasal sinuses. (a) Bilateral conchae bullosae (arrows). (b) Onodi cell on the left side (arrow), in close relation to the left optic nerve. (c) Paradoxical curvature of middle turbinate on the right side (arrow). (d) Supraorbital pneumatization, exposing bilateral anterior ethmoid arteries (thin arrows). The ethmoid air cells on the left side are opacified.*

## Paranasal sinuses

Non-contrast CT shows soft tissue density material with foci of hyperdensity, which represent calcium phosphate deposits concentrated in areas of mycelium necrosis [9]. (Figure 5). Unilateral soft tissue material in the sinonasal cavity is the most consistent early CT finding, although it is nonspecific [10].

On MRI, the mucosal thickening of sinuses usually appears isointense to grey matter on T1- and hyperintense on T2-weighted images. Sinus contents can show variable signals based on the nature of contents. Fungal elements appear hypointense on T2-weighted sequence due to the presence of heavy metals (Figure 6). Infection can extend into the intracranial compartment via the cribriform plate (Figure 9).

A crucial MRI finding is the black turbinate sign (Figure 7) [11]. Angioinvasive hyphae of mucor cause devitalization of mucosa, which appears as non-enhancing tissue on contrast-enhanced MRI (CE-MRI). It starts in the sinonasal mucosa, particularly the turbinates. On further spread, there is non-enhancement of extraocular muscles of the orbit (Figure 7) and palatal mucosa (Figure 8). However, benign turbinate nonenhancement can be seen in immunocompetent individuals as well, mostly attributed to sinusoids or capacitance vessels that can change size and cause temporary nonenhancement [12].


**Figure 5.** *Axial CT (a) at the level of the maxillary sinus and (b) at the level of the sphenoid sinus shows hyperdense contents within the left maxillary sinus (thin arrow), sphenoid sinus (black arrow), and left ethmoid air cells (thick arrow). (HU value: 70).*

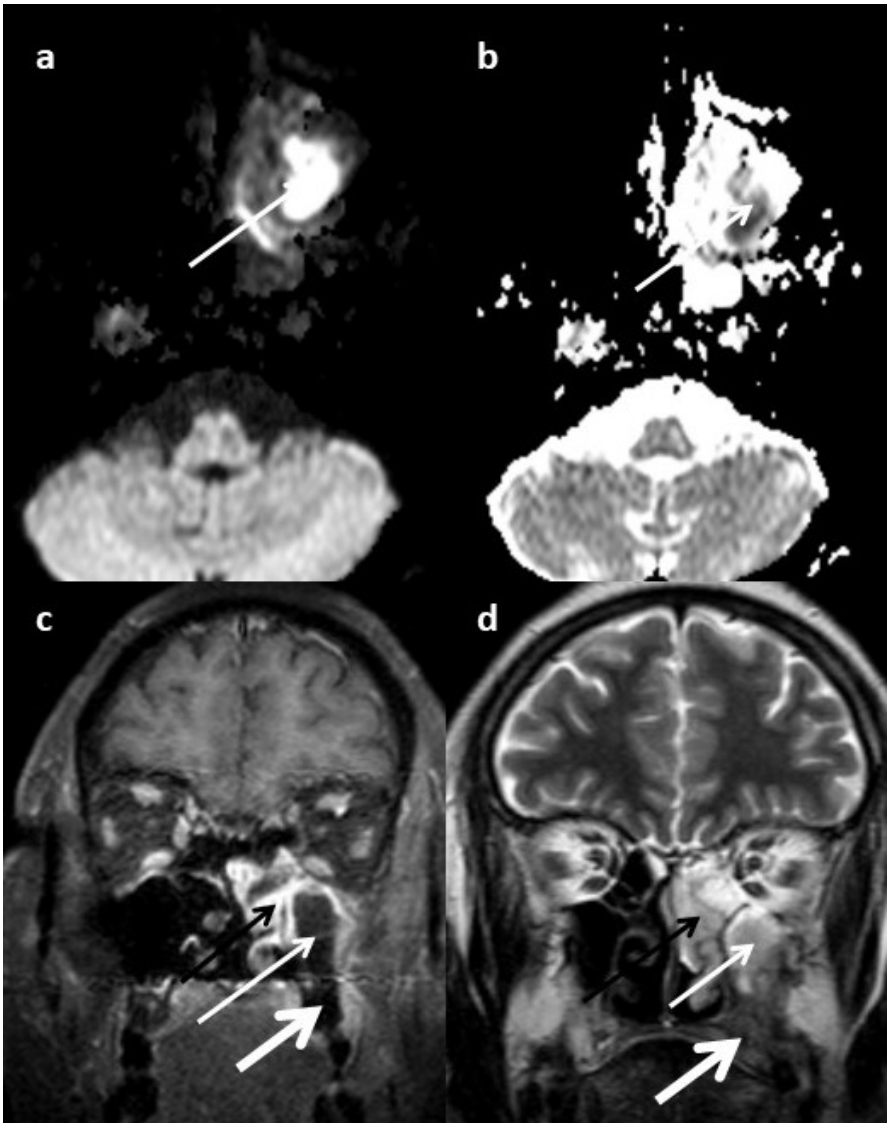


**Figure 6.** *(a) DWI (b) ADC map (c) Contrast-enhanced coronal image and (d) T2-weighted coronal images at the level of maxillary sinuses show peripherally enhancing mucosal hypertrophy with central non-enhancing contents in the left maxillary sinus (thin arrow). These show diffusion restriction and are seen to extend into the left nasal cavity (black arrow) and the alveolar process inferiorly (thick arrow).*

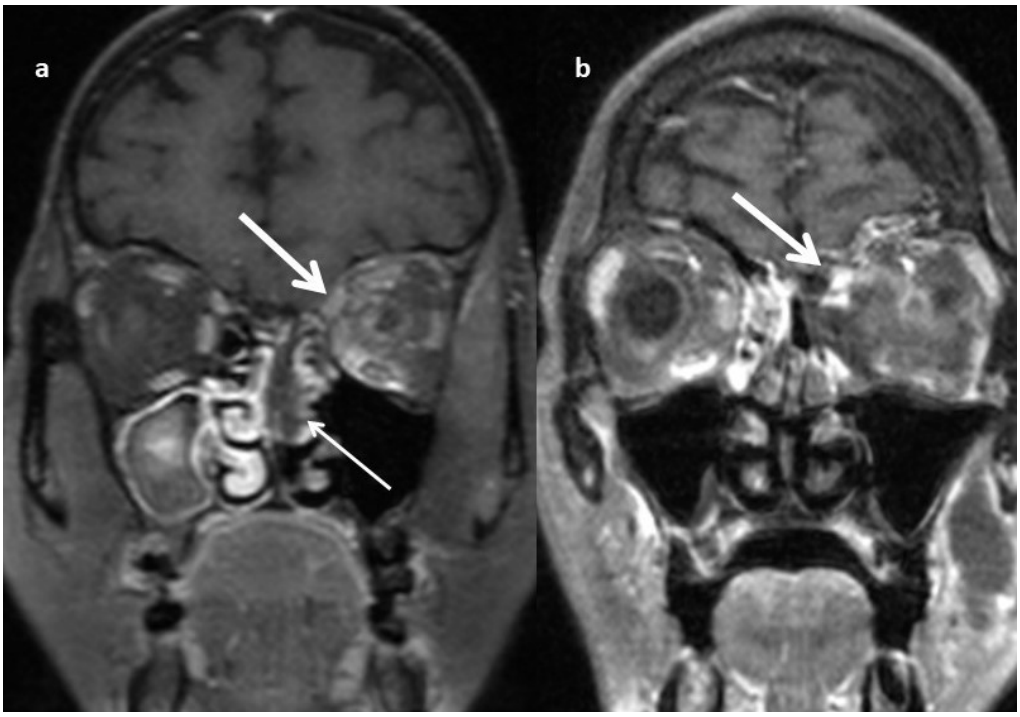


**Figure 7.** *(a) Coronal contrast-enhanced MRI (CEMRI) shows nonenhancement of middle turbinate on left side (black turbinate sign) (thin arrow). Peripherally enhancing contents with central nonenhancement is seen in the right maxillary sinus. Enhancing inflammatory tissue is seen involving the left superior oblique. (thick arrow). (b) Coronal contrast-enhanced MRI shows non-enhancement of medial rectus and superior oblique (thick arrow) with enhancement in intraconal fat. Non-enhancing tissue is seen involving periantral tissue on left side.*

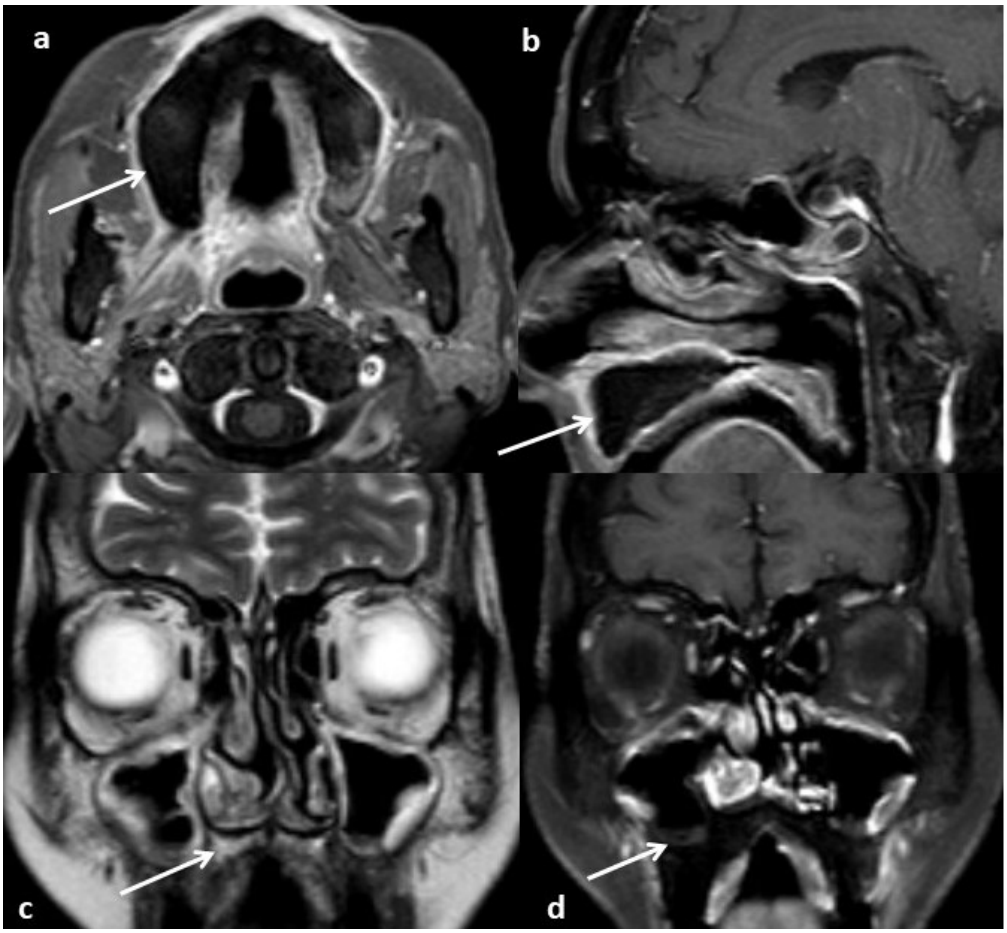


**Figure 8.** *(a) Axial contrast-enhanced MRI (b) Sagittal contrast-enhanced MRI (c) Coronal T2-weighted MRI and (d) Coronal contrast-enhanced MRI show expansion and nonenhancement of the alveolar process of the maxilla (predominantly on the right side) and the hard palate with peripheral soft tissue enhancement (arrows).*

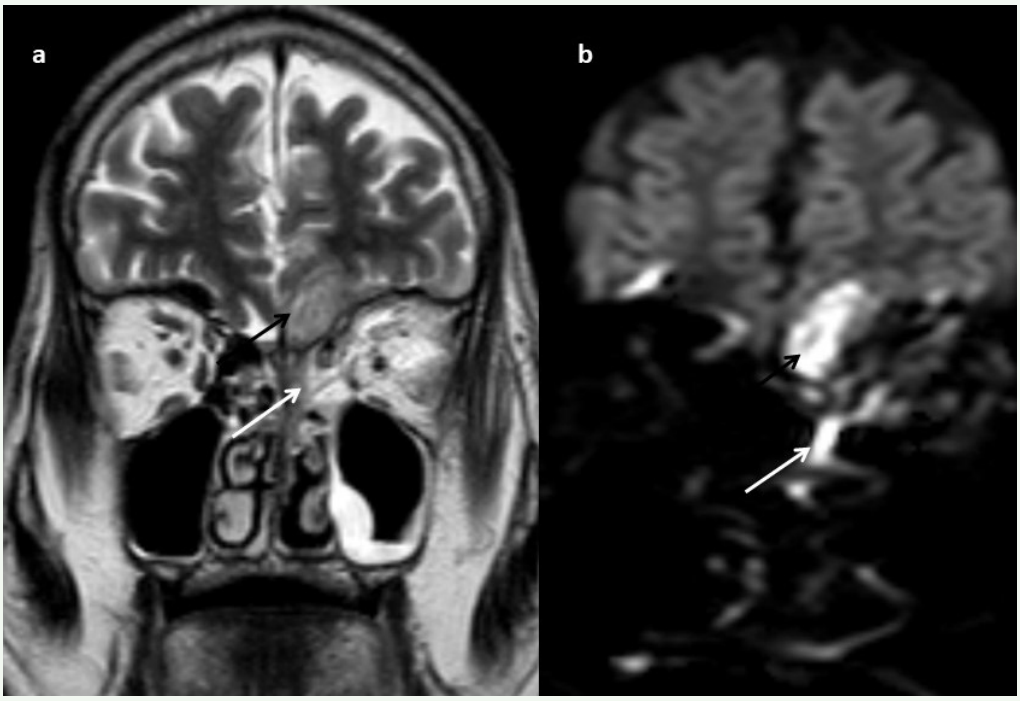


**Figure 9.** *(a) Coronal T2 weighted MRI and (b) Coronal DWI show extension of infection from ethmoid air cells (white arrows) to the gyrus rectus of the frontal lobe (black arrows), across the cribriform plate. The frontal lobe lesion and the ethmoid contents show intermediate signal intensity on T2-weighted image and restriction on DWI.*

## Oral and maxillofacial

Extrasinus spread can involve the neck spaces as well as the maxillofacial area up to the skull base (Figure 2,3,10). MRI is much more sensitive than the soft tissue algorithm of CT to detect extra-sinus spread, characterized by T2/FLAIR hyperintensity, with contrast enhancement interspersed with areas of nonenhancement indicating nonviable tissue [13].

Infection in the maxillary sinus can spread medially into the nasal cavity (Figure 6) and can involve the nasal septum and turbinates. Extension through the other walls involves the extracranial head and neck (Figure 10). Through the anterior wall of the maxillary sinus, the infection spreads to the pre-antral soft tissues (Figure 2). Retro-antral fat can be involved via the posterolateral wall of the maxillary sinus with extension to the infratemporal fossa (Figure 2).

The oral cavity can be involved via the hard palate or the alveolar process of the maxilla (Figure 6), and by perineural spread from the pterygopalatine fossa. (Figure 3). Perineural and perivascular spread occur, mostly along branches of the trigeminal nerve [14], sometimes along the labyrinthine segment of the facial nerve (Figure 3) [15].

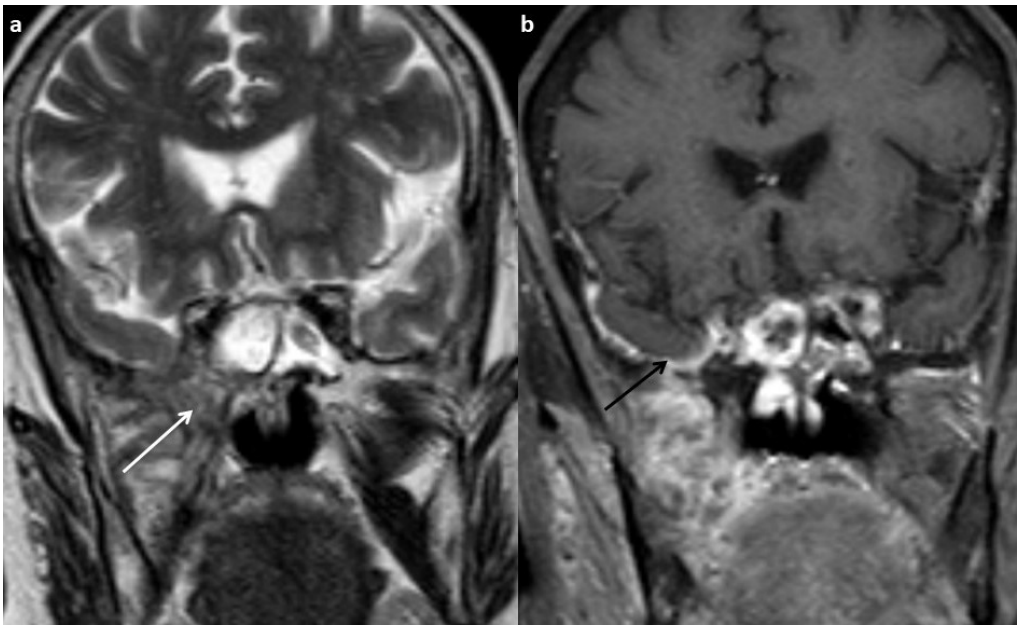


**Figure 10.** *(a) Coronal T2 weighted MRI and (b) Coronal CEMRI show loss of fat signal in the middle skull base on the right side indicative of skull base involvement (white arrow). The right infratemporal fossa and dura along the right temporal lobe show enhancement (black arrow).*

## Orbit

Involvement of the orbit can occur via the maxillary sinus, the pterygopalatine fossa, the lamina papyracea, the or nasolacrimal duct (Figure 1) [13]. NCCT findings include proptosis, thickening and blurring of margins of the optic nerve and extraocular muscles, and orbital fat stranding. Advanced cases can show fullness of the orbital apex (Figure 11).

On contrast studies, the extraocular muscles appear thickened and show a lack of normal contrast enhancement (Figure 7). The optic nerve can appear thickened, show non-enhancement, and sometimes can undergo infarction, showing diffusion restriction (Figure 12) [16]. One of the most dreaded complications of orbital mucormycosis is orbital compartment syndrome (Figure 13).

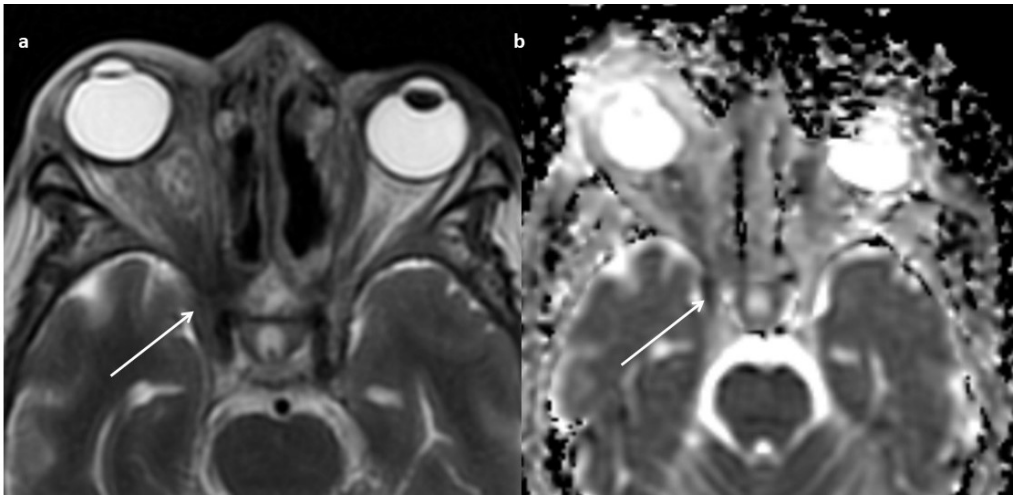


**Figure 11.** *(a) T2-weighted axial MRI showing involvement of intraconal fat and orbital apex on the right side with extension into cavernous sinus (arrow). (b) ADC map of the same patient shows diffusion restriction in the right cavernous sinus (arrow).*

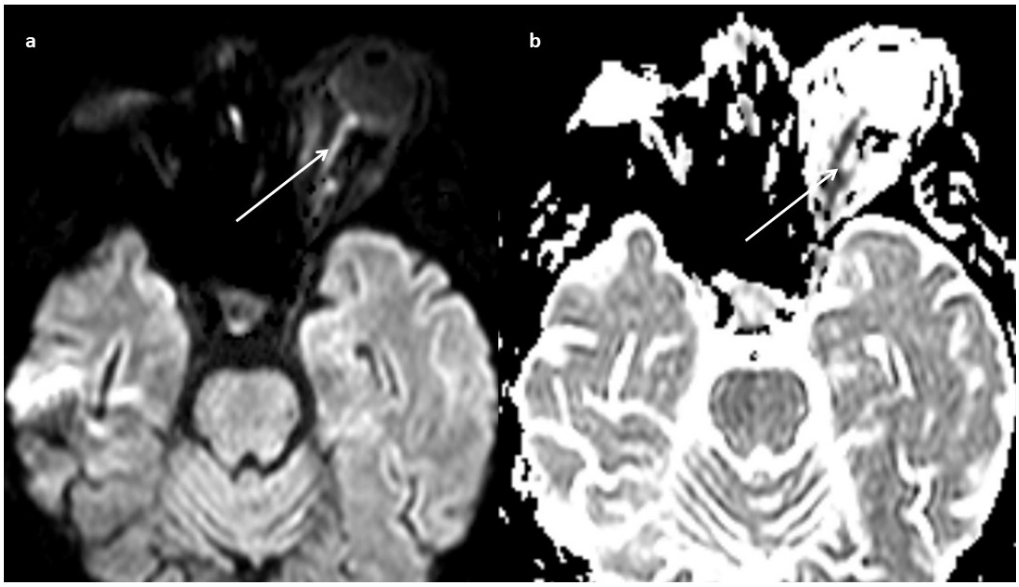


**Figure 12.** *Axial MRI (a) DWI and (b) ADC map show proptosis of the left globe and restricted diffusion in the left optic nerve (white and black arrow).*

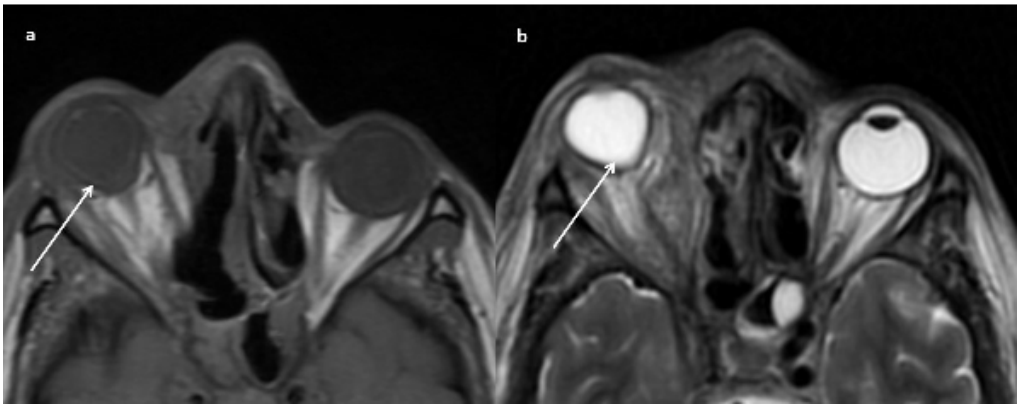


**Figure 13.** *Axial MRI of the orbit (a) T1-weighted (b) T2-weighted show proptosis, stretching of the optic nerve, and tenting of the globe (guitar pick sign) suggestive of orbital compartment syndrome (white arrows).*

## Brain

Intracranial spread occurs via the orbital apex or by direct extension of infection from the sinonasal compartment via the skull base. Osteomyelitis of the skull base manifests as low signal devitalized soft tissue in and around the bony skull base (Figure 10) [15].

Cavernous sinus thrombosis is one of the commonest intracranial manifestations, characterised by loss of flow void of internal carotid artery and nonenhancement on CEMRI (Figure 14).

Direct intracranial invasion can manifest as fungal abscesses. Restricted diffusion is a hallmark of pyogenic brain abscesses; however, findings in fungal abscesses are less specific (Figure 15) [17].

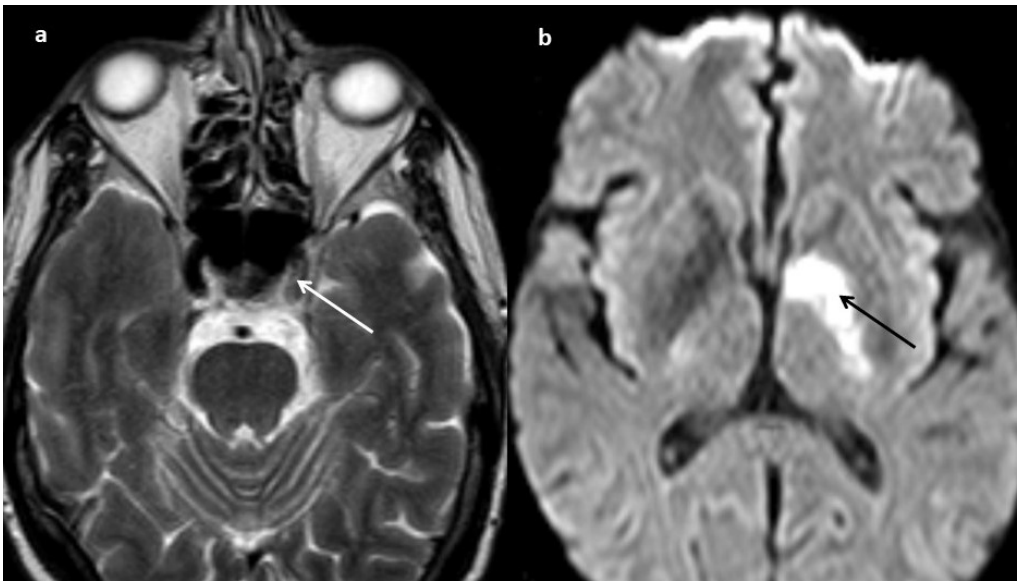


**Figure 14.** *(a) Axial T2-weighted MRI show loss of flow void of the left internal carotid artery (white arrow). (b) DWI of the same patient shows an acute infarct in the left gangliocapsular region (black arrow).*

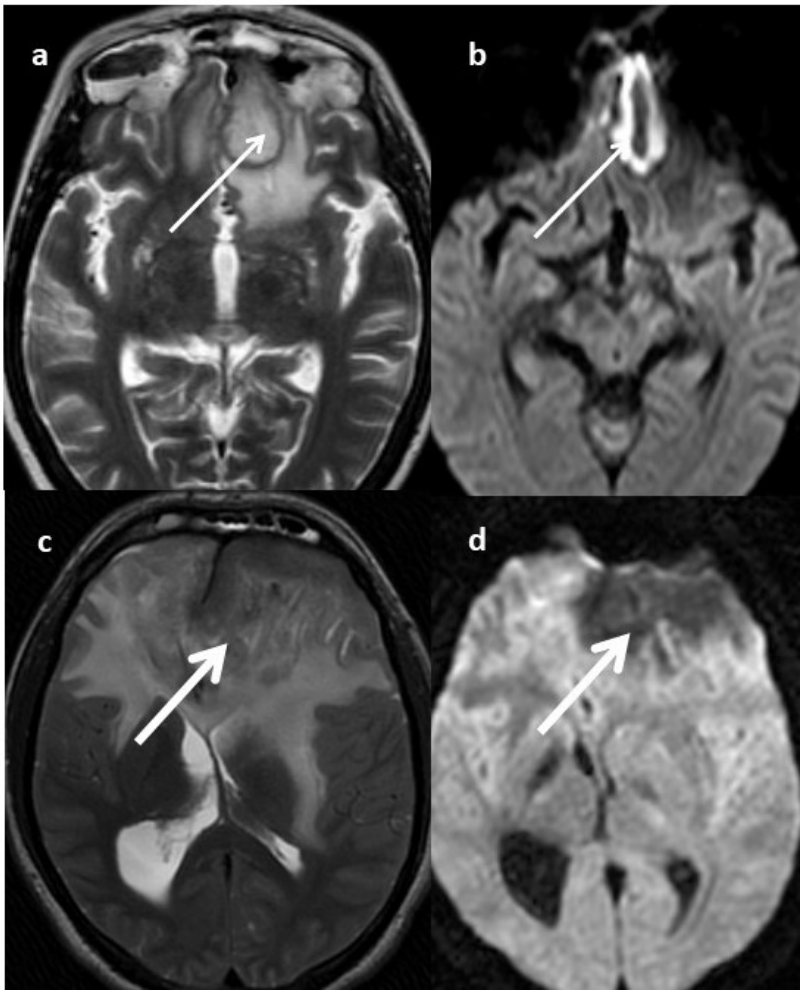


**Figure 15.** *Axial MRI (a) T2 weighted (b) DWI show a large lesion in the left gyrus rectus with peripheral restriction (thin arrows). Axial MRI (c) T2 weighted (d) DWI in another patient shows a large peripherally enhancing abscess in the left frontal lobe with no diffusion restriction (thick arrows).*

## Conclusion

Both CT and MRI play a vital role in the diagnosis and staging of mucormycosis. While CT gives excellent details of bony anatomy, particularly bony rarefaction, it has limitations in terms of assessment of soft tissue spread. MRI remains the mainstay in the assessment of the extent of spread and guide management.

## References

1. Roden MM, Zaoutis TE, Buchanan WL, Knudsen TA, Sarkisova TA, Schauflee RL, et al. Epidemiology and outcome of zygomycosis: a review of 929 reported cases. Clin Infect Dis 2005;41:634-53. doi: 10.1086/432579.

2. Chander J. Textbook of medical mycology. 4th ed. New Delhi: Jaypee Brothers Medical Publishers; 2018. p.554-96.

3. Kwon-Chung KJ. Taxonomy of fungi causing mucormycosis and entomophthoramycosis (zygomycosis) and nomenclature of the disease: molecular mycologic perspectives. Clin Infect Dis 2012;54 Suppl 1:S8-15. doi: 10.1093/cid/cir864.

4. Ibrahim AS, Spellberg B, Walsh TJ, Kontoyiannis DP. Pathogenesis of mucormycosis. Clin Infect Dis 2012;54 Suppl 1:S16-22. doi: 10.1093/cid/cir865.

5. Honavar SG. Code Mucor: guidelines for the diagnosis, staging and management of rhino-orbito-cerebral mucormycosis in the setting of COVID-19. Indian J Ophthalmol 2021;69:1361-5. doi: 10.4103/ijo.IJO_1165_21.

6. Singh AK, Singh R, Joshi SR, Misra A. Mucormycosis in COVID-19: a systematic review of cases reported worldwide and in India. Diabetes Metab Syndr 2021;15(4):102146. doi: 10.1016/j.dsx.2021.05.019.

7. O'Brien WT Sr, Hamelin S, Weitzel EK. The preoperative sinus CT: avoiding a "CLOSE" call with surgical complications. Radiology 2016;281:10-21. doi: 10.1148/radiol.2016152230.

8. Middlebrooks EH, Frost CJ, De Jesus RO, Massini TC, Schmalfuss IM, Mancuso AA. Acute invasive fungal rhinosinusitis: a comprehensive update of CT findings and design of an effective diagnostic imaging model. AJNR Am J Neuroradiol 2015 ;36:1529-35. doi: 10.3174/ajnr.A4298.

THE ASEAN JOURNAL OF RADIOLOGY
ISSN 2672-9393

9. Singh V. Fungal rhinosinisitis: unravelling the disease spectrum. J Maxillofac Oral Surg 2019;18:164-79. doi: 10.1007/s12663-018-01182-w.

10. Aribandi M, McCoy VA, Bazan C 3rd. Imaging features of invasive and noninvasive fungal sinusitis: a review. Radiographics 2007;27:1283-96. doi: 10.1148/rg.275065189.

11. Safder S, Carpenter JS, Roberts TD, Bailey N. The "Black Turbinate" sign: an early MR imaging finding of nasal mucormycosis. AJNR Am J Neuroradiol 2010;31:771-4. doi: 10.3174/ajnr.A1808.

12. Han Q, Escott EJ. The black turbinate sign, a potential diagnostic pitfall: evaluation of the normal enhancement patterns of the nasal turbinates. AJNR Am J Neuroradiol 2019;40:855-61. doi: 10.3174/ajnr.A6037.

13. Herrera DA, Dublin AB, Ormsby EL, Aminpour S, Howell LP. Imaging findings of rhinocerebral mucormycosis. Skull Base 2009;19:117-25. doi: 10.1055/s-0028-1096209.

14. Sravani T, Uppin SG, Uppin MS, Sundaram C. Rhinocerebral mucormycosis: pathology revisited with emphasis on perineural spread. Neurol India 2014;62:383-6. doi: 10.4103/0028-3886.141252.

15. Sanghvi D, Kale H. Imaging of COVID-19-associated craniofacial mucormycosis: a black and white review of the "black fungus". Clin Radiol 2021;76:812-9. doi: 10.1016/j.crad.2021.07.004.

16. Hatipoglu HG, Gurbuz MO, Yuksel E. Restricted diffusion in the optic nerve and retina demonstrated by MRI in rhino-orbital mucormycosis. J Neuroophthalmol 2009 ;29:13-5. doi: 10.1097/WNO.0b013e318183bde4.

17. Gaviani P, Schwartz RB, Hedley-Whyte ET, Ligon KL, Robicsek A, Schaefer P, et al. Diffusion-weighted imaging of fungal cerebral infection. AJNR Am J Neuroradiol 2005 ;26:1115-21.

ASEAN Movement in Radiology

# Multidisciplinary working group for interstitial lung disease in Thailand: Part 2 – a concise review of published visual scoring methods for interstitial lung disease

*Juntima Euathrongchit, M.D.*[(1)]
*Phakphoom Thiravit, M.D.*[(2)]
*Wiwatana Tanomkiat, M.D.*[(3)]
*Chayanin Nitiwarangkul, M.D.*[(4)]
*Thanisa Tongbai, M.D.*[(5)]
*Yutthaphan Wannosopha, M.D.*[(1)]
*Thitiporn Suwatanapongched, M.D.*[(4)]

From [(1)] Department of Radiology, Faculty of Medicine, Chiangmai University, Chiangmai, Thailand
[(2)] Department of Radiology, Siriraj Hospital, Mahidol University, Bangkok, Thailand
[(3)] Department of Radiology, Faculty of Medicine, Prince of Songkla University, Songkla, Thailand,
[(4)] Department of Diagnostic and Therapeutic Radiology, Faculty of Medicine Ramathibodi Hospital, Mahidol University, Bangkok, Thailand,
[(5)] Department of Radiology, Faculty of Medicine, Chulalongkorn University, Bangkok, Thailand.

Address correspondence to J.E. (e-mail: juntima.eua@cmu.ac.th )

Received 5 April 2022 ; accepted 6 April 2022
doi:10.46475/aseanjr.v23i1.170

**Keywords:** Interstitial lung disease, Fibrotic extent, Disease extent, Multidisciplinary discussion, Thailand.

THE ASEAN JOURNAL OF RADIOLOGY
ISSN 2672-9393

## Introduction

Interstitial lung disease (ILD) comprises a large group of multiple disorders causing a variable degree of inflammatory and fibrotic changes predominantly in the interstitial parts of the lungs [1]. Two main histopathological changes of ILDs [2, 3] consist of usual interstitial pneumonia (UIP) and nonspecific interstitial pneumonia (NSIP). UIP representing advanced pulmonary fibrosis is typically found in idiopathic pulmonary fibrosis (IPF). Although NSIP is the most common histopathology in ILD associated with a connective tissue disease (CTD), other histopathological changes, including UIP, can also be found.

On HRCT, the presence of clustered subpleural cystic air spaces reflecting honeycombing and immediate subpleural sparing is considered the hallmark for UIP (Figure 1A) and NSIP (Figure 1B), respectively [3, 4]. However, differentiating bronchiectasis and bronchiolectasis seen in NSIP from subpleural honeycombing in UIP are sometimes crucially problematic. Due to clinical overlap and HRCT features of UIP and NSIP, the diagnosis and treatment of ILD are sometimes not straightforward. A correct diagnosis leading to a successful treatment requires a combination of clinical information (thorough clinical history taking and physical examination), laboratory data, HRCT findings, and sometimes lung biopsy for histopathological information through a multidisciplinary discussion (MDD).

HRCT is considered an essential part of MDD. An accurate interpretation of the disease pattern, the disease extent, and the presence and degree of lung fibrosis, could guide the disease etiology and diagnosis. Moreover, the degree of the disease extent and fibrotic severity could reflect treatment success and prognosis.

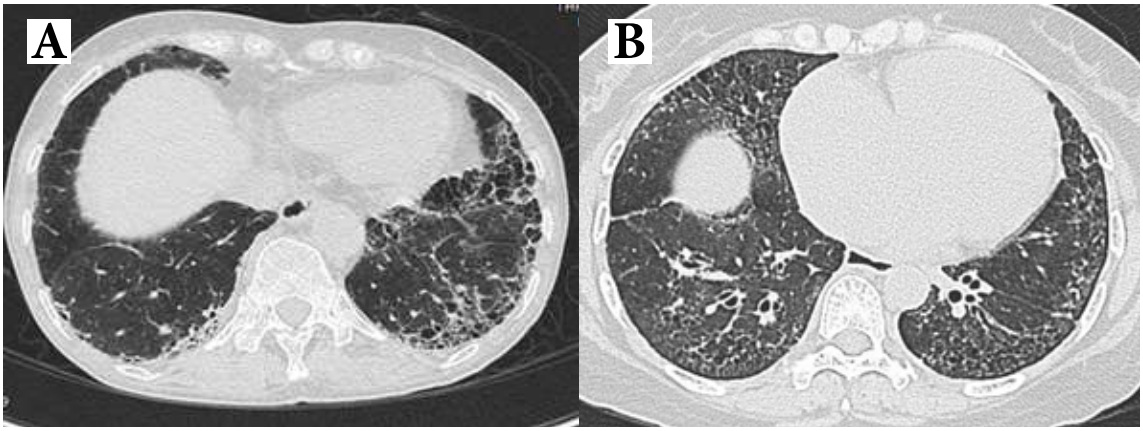


**Figure 1.** *Axial HRCT at basal lung (A) in UIP pattern showing subpleural honeycombing in bilateral basal lungs with slightly asymmetric involvement. Axial HRCT at the level of the right dome of diaphragm. (B) in the fibrotic NSIP pattern showing mixed ground-glass and reticular opacities with traction bronchiectasis, traction bronchiolectasis, architectural distortion, relative sparing of the immediate lungs, and symmetric involvement.*

## Scoring system

Since the disease severity is essential for the current treatment guideline [1], HRCT has become the cornerstone CT for diagnosing and properly managing ILDs, particularly those associated with CTD and IPF. In addition, it helps select patients who will benefit from the antifibrotic therapy. An accurate estimation of the disease and fibrotic extents of ILD is therefore mandatory.

In the past two decades, many published scoring methods have been based on visual estimation of the disease severity and lung fibrosis on HRCT, especially those with IPF and CTD-ILD [5-12]. These methods can be categorized into comparative and semi-quantitative scoring methods. Noteworthly, there are substantial differences among these methods regarding the number of the sampling lung levels or lung zones, the percentage or grading for estimating the extent of involvement, and the weighting factors due to the concern of the unequal lung areas [11, 13]. Table 1 summarizes published visual scoring methods for ILDs commonly adopted in research and clinical practice.

As shown in Table 1, the sampling lung from the lung apex to the lung base ranged from three to five anatomical levels based on axial HRCT images, and the exact anatomical lung levels or zones used are also different (Figure 2). Nevertheless, the lung level was preferred in most previous studies since it is easy to localize without being accustomed to the anatomical boundary of the lung lobe on CT images. For the three-level method, Sánchez et al. [8] selected the anatomical level in each lung zone showing the most extensive involvement for estimating the disease extent.

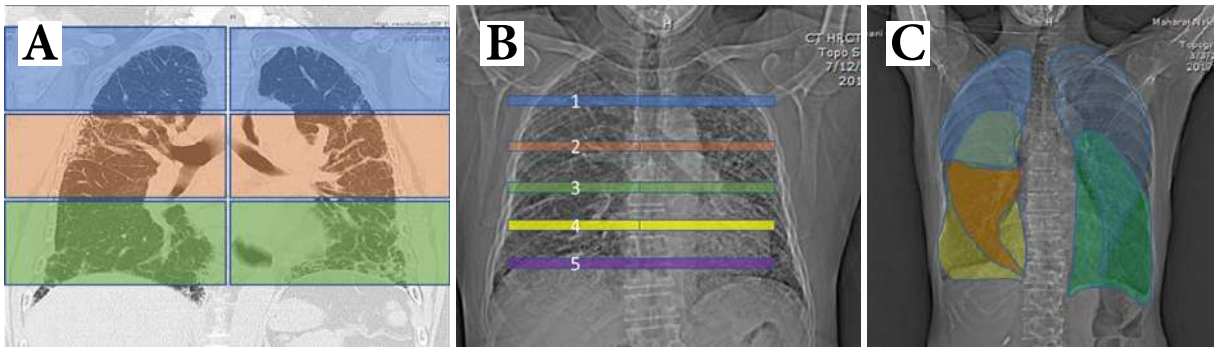


**Figure 2.** *Illustrations for the published visual CT scoring methods (A) three-level method (B) five-level method, and (C) five lung lobes.*

**Table 1.** *Summary of the published visual scoring methods for ILD.*

| Authors (year), methods & keys | Abnormality and grading | Predefined anatomical levels or zones for evaluation | Adopted by | Advantages |
|---|---|---|---|---|
| Wells et al. [14] (1992)<br>Comparative scoring<br><br>Keys:<br>- Score: Grade<br>- Parenchymal disease extent on HRCT correlated with lung histology | Severity grading<br>1 = Parenchymal opacity alone<br>2 = Parenchymal opacity > reticulation pattern extent<br>3 = Parenchymal opacity = reticular pattern extent<br>4 = Reticular pattern extent > parenchymal opacity<br>5 = Reticular pattern alone<br><br>Maximum score = 5 per lobe | Five lung lobes | Pignone et al. [15];<br>Davas et al. [16];<br>Shahin et al. [17];<br>Giacomelli et al. [18];<br>Shah et al. [19];<br>Gohari et al. [20] | - Correlation of high score and fibrotic specimen or low score and inflammatory specimen<br>- Parenchymal disease extent on HRCT correlated with lung histology |
| Warrick et al. [11] (1991)<br>Semi-quantitative scoring<br><br>Keys:<br>- Score: Grade<br>- Combination of severity and extent of disease compared with clinical context | Severity grading based on HRCT features in each bronchopulmonary segment<br>1 = GGO<br>2 = Irregular pleural margin<br>3 = Septal or subpleural line<br>4 = Honeycombing<br>5 = Subpleural cyst<br><br>Extent grading based on the number of bronchopulmonary segments involved<br>- 1 to 3 segments = 1<br>- 4 to 9 segments = 2<br>- > 9 segments = 3 | Bronchopulmonary segments | Bellia et al. [5];<br>Diot E et al. [21];<br>Orlandi I et al. [22];<br>Afeltra et al. [23];<br>Camiciottoli et al. [24];<br>Yiannopoulos et al.[25];<br>Savarino et al.[26];<br>Daoussis D et al.[27] | - Total score correlated inversely with total lung capacity, diffusion lung capacity for carbon monoxide, and forced expiratory volume in 1 second<br>- Alveolitis and fibrosis, two keys from HRCT |
| Kazerooni EA et al. [7] (1997) and Ooi GC et al. [28] (2003)<br><br>Semi-quantitative scoring<br>Keys:<br>- Score: Grade<br>- Evaluation of extent and severity of disease | Abnormality<br>- GGO alone<br>- Mixed GGO and reticulation<br>- Reticular fibrosis alone<br>- Honeycombing<br><br>Extent grade by area of disease involvement in one lobe<br>1 = involved 1 –25%<br>2 = involved 26 – 50%<br>3 = involved 51 – 75%<br>4 = involved > 75% | Lobes are scored independently<br>Lingula is considered a separate lobe: 6 total lobes<br><br>Anatomical landmark<br>- Arch<br>- Carina<br>- 1 cm above diaphragm | Choi et al. [29];<br>Mok et al. [30];<br>Pandey et al. [31];<br>Tiev et al. [32] | Fibrosis score was high as 25<br>- Cellularity score and desquamation score was about 10<br>- Granulation score was about 9 |
| Goldin et al. [33] (2009)<br>Semi-quantitative scoring;<br>Scleroderma Lung Study (SLS)<br><br>Keys:<br>- Score: Grade<br>- Evaluation of extent and severity of disease | Abnormality in each each lung zone<br>- GGO alone<br>- Fibrosis (thick reticulation)<br>- Bronchiectasis/ bronchiolectasis<br>- Honeycombing<br><br>Extent grade based on percentage of involvement in each zone<br>1 = involved 1– 25%<br>2 = involved 26 – 50%<br>3 = involved 51 – 75%<br>4 = involved > 75% | hree lung zones of each lung are scored for each abnormality<br>- Zone 1: Apex to aortic arch<br>- Zone 2: Aortic arch to inferior pulmonary veins<br>- Zone 3: Inferior pulmonary veins to diaphragm | Scleroderma Lung Study (SLS) | - Lung fibrosis and GGO were commonest imaging findings in symptomatic systemic sclerosis (SSc) patients.<br>- No relationship between progression and baseline lung fibrosis; or limited SSc vs. diffuse SSc. |

| Authors (year), methods & keys | Abnormality and grading | Predefined anatomical levels or zones for evaluation | Adopted by | Advantages |
|---|---|---|---|---|
| Well et al. [34] (1997)<br>Quantitative and semi-quantitative scoring<br><br>Keys:<br>- Score: percentage<br>- Evaluation<br>1. Global disease extent<br>2. Reticulation extent<br>3. Percentage of GGO | 1. Global disease extent – estimated to the nearest 5 %<br>2. % of GGO: proportion of total disease extent<br>3. Extent of reticulation: proportion of toral disease extent<br>4. Coarseness of reticulation (fibrotic severity)<br><br>0 = Normal<br>1 = Fine intralobular fibrosis<br>2 = Microcystic honeycombing<br>3 = Macrocystic honeycombing<br><br>The total disease extent is composed of the mean of the percentage of disease at each level | Anatomic landmark (multiplied with weight factor)<br>1) Origin of the great vessels<br>2) Main carina<br>3) Pulmonary venous confluence<br>4) Halfway between levels 3 and 5<br>5) Immediately above right hemidiaphragm | Goh et al. [6];<br>Desai et al. [35];<br>Hoyles et al. [36] | Goh et al. showed the global extent of disease<br>> 20% → significantly increased mortality of SSc. |
| Euathrongchit et al. (2014)<br>CMU scleroderma score [9, 10]<br><br>Keys:<br>- Score: Grade<br>- Evaluation of extent and severity of disease<br>1. GGO<br>2. Reticulation<br>3.Traction bronchiectasis<br>4. Honeycombing | Determine the grade of each abnormality based on the percentage of lung involvement in each lobe<br>1 = involved 1 – 25%<br>2 = involved 26 – 50%<br>3 = involved 51 – 75%<br>4 = involved > 75% | Five lung lobes | Wangkaew et al. [9, 10] | - Thai patients<br>- Sensitive method for monitoring disease |

Despite the substantial difference in the scoring methods, all of them provided good interobserver agreements and inter-rater reliability, especially when performed by chest radiologists (interobserver agreement kappa 0.74 – 0.88 for overall grading and fibrosis grading, respectively [37]).

With modern CT technology and a simplified method for radiologists, rheumatologists and chest physicians to use a scoring system, we recommended evaluating the disease extent in the global disease and the amount of fibrosis. A semi-quantitative method estimated the amount of the global disease and the fibrotic extent in each reference image in percentage and calculate the average percentage. The reference images could be either 3 or 5 levels, Figure 3 and Table 2 are examples. Moreover, since IPF and the CTD-ILD disease mainly involved the basal lung, we encouraged the evaluation of the sulcal areas for weight as well (see detail in part 3 [38]) and more structural references that facilitated the usage by trainees, general radiologists and physicians.

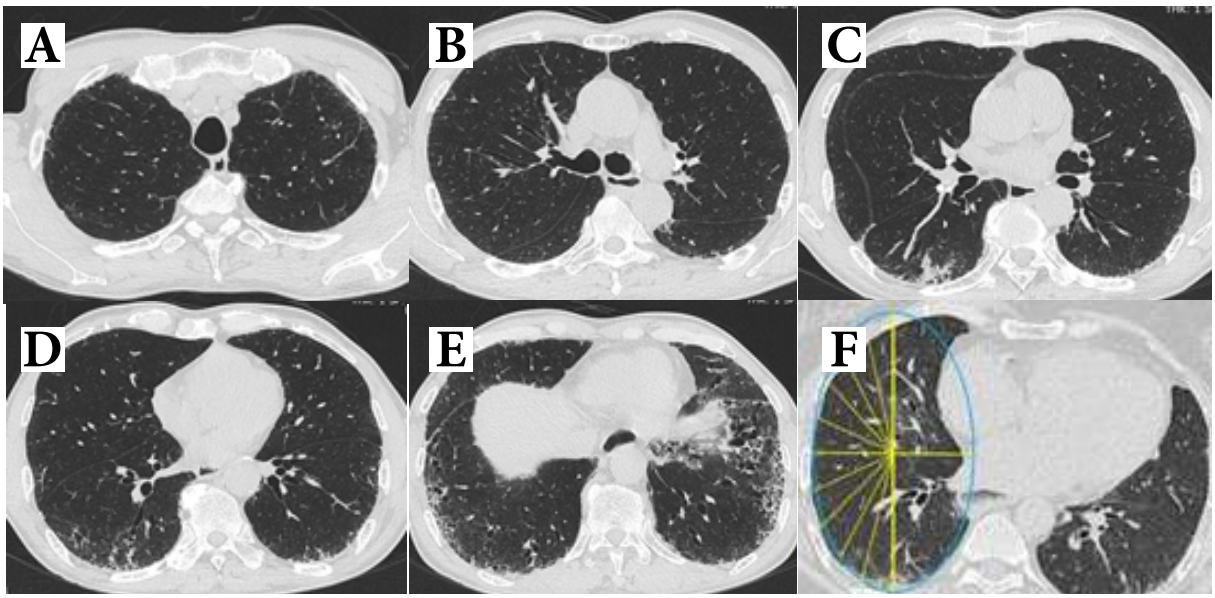


**Figure 3.** *Axial HRCT (A – E) 5 level from upper to lower lung fields. (A) the origin of great vessels, (B) the carina, (C) the pulmonary venous confluence, (D) between C and E and (E ) the right hemidiaphargm level, respectively. Each right or left lung area is about 100% and divided uniformly into small pieces as small as about 5% area (F) that are used to estimate amount of disease findings. The estimated global disease extent and fibrotic extent are summarized in Table 2.*

**Table 2.** *Summary of the global disease extent and the fibrotic extent calculation by the previously published methods (three–level and five–level methods).*

| Area reference | Global disease extent (%) | | Fibrotic extent (%) | | Average of the summed global disease extent | Average of the summed fibrotic extent |
|---|---|---|---|---|---|---|
| | Rt | Lt | Rt | Lt | | |
| Three-level method by Kazerooni EA et al. [7]; Ooi GC et al. [28] and Goldin et al. [33] | | | | | | |
| L1 above arch | 5 | 5 | 5 | 5 | | |
| L2 arch to vascular confluence | 20 | 10 | 15 | 10 | 20-25% [(140x100)/600 =23.3] | 20-25% [(135x100)/600 =22.5] |
| L3 below vascular confluence | 40 | 60 | 35 | 55 | | |
| Five–level method by Goh et al. [6] and Well et al. [34] | | | | | | |
| L1 great vessel origin | 5 | 5 | 5 | 5 | | |
| L2 carina | 0 | 5 | 0 | 5 | 20% [(195x100)/1000 =19.5] | 15-20% [(170x100)/1000 =17] |
| L3 vascular confluence | 20 | 5 | 15 | 5 | | |
| L4 between L3&L5 | 25 | 10 | 20 | 10 | | |
| L5 diaphragm | 50 | 70 | 45 | 60 | | |

## References

1. Tanomkiat W, Nitiwarangkul C, Euathrongchit J, Thiravit P, Tongbai T, Suwatanapongched T. Multidisciplinary working group for interstitial lung disease in Thailand: Part 1- rationale in developing a guide to estimate the global disease and fibrotic extents on high-resolution computed tomography. ASEAN J Radiol [Internet]. 2021 [cited 2021 Apr 1];22(3):47-60. Available from: https://www.asean-journal-radiology.org/index.php/ajr/article/view/158/106

2. Lynch DA, Sverzellati N, Travis WD, Brown KK, Colby TV, Galvin JR, et al. Diagnostic criteria for idiopathic pulmonary fibrosis: a Fleischner Society White Paper. Lancet Respir Med 2018;6:138-53. doi: 10.1016/S2213-2600(17)30433-2.

3. Raghu G, Remy-Jardin M, Myers JL, Richeldi L, Ryerson CJ, Lederer DJ, et al. Diagnosis of idiopathic pulmonary fibrosis. an official ATS/ERS/JRS/ALAT clinical practice guideline. Am J Respir Crit Care Med 2018;198(5):e44-e68. doi: 10.1164/rccm.201807-1255ST.

4. Galhotra RD, Singh G, Saggar K, Saggar K, Gupta K. Primary thoracic manifestations in connective tissue diseases on high resolution computed to mography: a prospective study. IJCMSR 2018;3:25-35.

5. Bellia M, Cannizzaro F, Scichilone N, Riili M, Triolo G, Midiri M, et al. HRCT and scleroderma: semiquantitative evaluation of lung damage and functional abnormalities. Radiol Med 2009;114:190-203. doi: 10.1007/s11547-009-0367-9.

6. Goh NS, Desai SR, Veeraraghavan S, Hansell DM, Copley SJ, Maher TM, et al. Interstitial lung disease in systemic sclerosis: a simple staging system. Am J Respir Crit Care Med 2008;177:1248-54. doi: 10.1164/rccm.200706-877OC.

7. Kazerooni EA, Martinez FJ, Flint A, Jamadar DA, Gross BH, Spizarny DL, et al. Thin-section CT obtained at 10-mm increments versus limited three-level thin-section CT for idiopathic pulmonary fibrosis: correlation with pathologic scoring. AJR Am J Roentgenol 1997;169:977-83. doi: 10.2214/ajr.169.4.9308447.

8. Sánchez RP, Fernández-Fabrellas E, Samper GJ, Montañana ML, Vilar LN. Visual HRCT score to determine severity and prognosis of idiopathic pulmonary fibrosis. Int J Respir Pulm Med 2018;5:084. doi:10.23937/2378-3516/1410084

9. Wangkaew S, Euathrongchit J, Patiwetwitoon S, Prasertwitayakij N, Kasitanon N, Louthrenoo W. The relevance of high-resolution computed tomographic findings and pulmonary arterial hypertension in systemic sclerosis-associated interstitial lung disease. J Med Assoc Thai 2014;97:878-85.

10. Wangkaew S, Euathrongchit J, Wattanawittawas P, Kasitanon N, Louthrenoo W. Incidence and predictors of interstitial lung disease (ILD) in Thai patients with early systemic sclerosis: Inception cohort study. Mod Rheumatol 2016;26:588-93. doi: 10.3109/14397595.2015.1115455.

11. Warrick JH, Bhalla M, Schabel SI, Silver RM. High resolution computed tomography in early scleroderma lung disease. J Rheumatol 1991;18:1520-8.

12. Zisman DA, Karlamangla AS, Ross DJ, Keane MP, Belperio JA, Saggar R, et al. High-resolution chest CT findings do not predict the presence of pulmonary hypertension in advanced idiopathic pulmonary fibrosis. Chest 2007;132:773-9. doi: 10.1378/chest.07-0116.

13. Wells AU, Rubens MB, du Bois RM, Hansell DM. Serial CT in fibrosing alveolitis: prognostic significance of the initial pattern. AJR Am J Roentgenol 1993;161:1159-65. doi: 10.2214/ajr.161.6.8249719.

14. Wells AU, Hansell DM, Corrin B, Harrison NK, Goldstraw P, Black CM, et al. High resolution computed tomography as a predictor of lung histology in systemic sclerosis. Thorax 1992;47:738-42. doi: 10.1136/thx.47.9.738.

15. Pignone A, Matucci-Cerinic M, Lombardi A, Fedi R, Fargnoli R, De Dominicis R, et al. High resolution computed tomography in systemic sclerosis. Real diagnostic utilities in the assessment of pulmonary involvement and comparison with other modalities of lung investigation. Clin Rheumatol 1992;11:465-72. doi: 10.1007/BF02283100.

16. Davas EM, Peppas C, Maragou M, Alvanou E, Hondros D, Dantis PC. Intravenous cyclophosphamide pulse therapy for the treatment of lung disease associated with scleroderma. Clin Rheumatol 1999;18:455-61. doi: 10.1007/s100670050138.

17. Shahin AA, Sabri YY, Mostafa HA, Sabry EY, Hamid MA, Gamal H, et al. Pulmonary function tests, high-resolution computerized tomography, alpha1-antitrypsin measurement, and early detection of pulmonary involvement in patients with systemic sclerosis. Rheumatol Int 2001;20:95-100. doi: 10.1007/s002960000089.

18. Giacomelli R, Valentini G, Salsano F, Cipriani P, Sambo P, Conforti ML, et al. Cyclophosphamide pulse regimen in the treatment of alveolitis in systemic sclerosis. J Rheumatol 2002;29:731-6.

19. Shah RM, Jimenez S, Wechsler R. Significance of ground-glass opacity on HRCT in long-term follow-up of patients with systemic sclerosis. J Thorac Imaging 2007;22:120-4. doi: 10.1097/01.rti.0000213572.16904.40.

20. Gohari Moghadam K, Gharibdoost F, Parastandechehr G, Salehian P. Assessments of pulmonary involvement in patients with systemic sclerosis. Arch Iran Med 2011;14:22-6.

21. Diot E, Boissinot E, Asquier E, Guilmot JL, Lemarie E, Valat C, et al. Relationship between abnormalities on high-resolution CT and pulmonary function in systemic sclerosis. Chest 1998;114:1623-9. doi: 10.1378/chest.114.6.1623.

22. Orlandi I, Camiciottoli G, Diciotti S, Bartolucci M, Cavigli E, Nacci F, et al. Thin-section and low-dose volumetric computed tomographic densitometry of the lung in systemic sclerosis. J Comput Assist Tomogr 2006;30:823-7. doi: 10.1097/01.rct.0000228159.86096.47.

23. Afeltra A, Zennaro D, Garzia P, Gigante A, Vadacca M, Ruggiero A, et al. Prevalence of interstitial lung involvement in patients with connective tissue diseases assessed with high-resolution computed tomography. Scand J Rheumatol 2006;35:388-94. doi: 10.1080/03009740600844381.

24. Camiciottoli G, Orlandi I, Bartolucci M, Meoni E, Nacci F, Diciotti S, et al. Lung CT densitometry in systemic sclerosis: correlation with lung function, exercise testing, and quality of life. Chest 2007;131:672-81. doi: 10.1378/chest.06-1401.

25. Yiannopoulos G, Pastromas V, Antonopoulos I, Katsiberis G, Kalliolias G, Liossis SN, et al. Combination of intravenous pulses of cyclophosphamide and methylprednizolone in patients with systemic sclerosis and interstitial lung disease. Rheumatol Int 2007;27:357-61. doi: 10.1007/s00296-006-0217-1.

26. Savarino E, Bazzica M, Zentilin P, Pohl D, Parodi A, Cittadini G, et al. Gastroesophageal reflux and pulmonary fibrosis in scleroderma: a study using pH-impedance monitoring. Am J Respir Crit Care Med 2009;179:408-13. doi: 10.1164/rccm.200808-1359OC.

27. Daoussis D, Liossis SN, Tsamandas AC, Kalogeropoulou C, Kazantzi A, Sirinian C, et al. Experience with rituximab in scleroderma: results from a 1-year, proof-of-principle study. Rheumatology (Oxford) 2010;49:271-80. doi: 10.1093/rheumatology/kep093.

28. Ooi GC, Mok MY, Tsang KW, Wong Y, Khong PL, Fung PC, et al. Interstitial lung disease in systemic sclerosis. Acta Radiol 2003;44:258-64. doi: 10.1034/j.1600-0455.2003.00058.x.

29. Choi HJ, Shin YK, Lee HJ, Kee JY, Shin DW, Lee EY, et al. The clinical significance of serum N-terminal pro-brain natriuretic peptide in systemic sclerosis patients. Clin Rheumatol 2008;27:437-42. doi: 10.1007/s10067-007-0724-9.

30. Mok MY, Fung PC, Ooi C, Tse HF, Wong Y, Lam YM, et al. Serum nitric oxide metabolites and disease activity in patients with systemic sclerosis. Clin Rheumatol 2008;27:315-22. doi: 10.1007/s10067-007-0708-9.

31. Pandey AK, Wilcox P, Mayo JR, Sin D, Moss R, Ellis J, et al. Predictors of pulmonary hypertension on high-resolution computed tomography of the chest in systemic sclerosis: a retrospective analysis. Can Assoc Radiol J 2010;61:291-6. doi: 10.1016/j.carj.2010.02.006.

32. Tiev KP, Cabane J, Aubourg F, Kettaneh A, Ziani M, Mouthon L, et al. Severity of scleroderma lung disease is related to alveolar concentration of nitric oxide. Eur Respir J 2007;30:26-30. doi: 10.1183/09031936.00129806.

33. Goldin J, Elashoff R, Kim HJ, Yan X, Lynch D, Strollo D, et al. Treatment of scleroderma-interstitial lung disease with cyclophosphamide is associated with less progressive fibrosis on serial thoracic high-resolution CT scan than placebo: findings from the scleroderma lung study. Chest 2009;136:1333-40. doi: 10.1378/chest.09-0108.

34. Wells AU, Hansell DM, Rubens MB, King AD, Cramer D, Black CM, et al. Fibrosing alveolitis in systemic sclerosis: indices of lung function in relation to extent of disease on computed tomography. Arthritis Rheum 1997;40:1229-36. doi: 10.1002/1529-0131(199707)40:7<1229::AID-ART6>3.0.CO;2-W.

THE ASEAN JOURNAL OF RADIOLOGY
ISSN 2672-9393

35. Desai SR, Veeraraghavan S, Hansell DM, Nikolakopolou A, Goh NS, Nicholson AG, et al. CT features of lung disease in patients with systemic sclerosis: comparison with idiopathic pulmonary fibrosis and nonspecific interstitial pneumonia. Radiology 2004;232:560-7. doi: 10.1148/radiol.2322031223.

36. Hoyles RK, Ellis RW, Wellsbury J, Lees B, Newlands P, Goh NS, et al. A multicenter, prospective, randomized, double-blind, placebo-controlled trial of corticosteroids and intravenous cyclophosphamide followed by oral azathioprine for the treatment of pulmonary fibrosis in scleroderma. Arthritis Rheum 2006;54:3962-70. doi: 10.1002/art.22204.

37. Assayag D, Kaduri S, Hudson M, Hirsch A, Baron M. High resolution computed tomography scoring systems for evaluating interstitial lung disease in systemic sclerosis patients. Rheumatology 2012;S1:003. Doi: 10.4172/2161-1149.S1-003

38. Suwatanapongched T, Nitiwarangkul C, Euathrongchit J, Thiravit P, Tongbai T,Tanomkiat W. Multidisciplinary working group for interstitial lung disease in Thailand: Part 3- proposed visual scoring method for quantifying the global disease and fibrotic extents on high-resolution CT. ASEAN J Radiol In press 2022.

ASEAN Movement in Radiology

# Multidisciplinary working group for interstitial lung disease in Thailand: Part 3 – the proposed visual scoring method for quantifying the global disease and fibrotic extents on high-resolution CT

*Thitiporn Suwatanapongched, M.D.*[(1)]
*Chayanin Nitiwarangkul, M.D.*[(1)]
*Juntima Euathrongchit, M.D.*[(2)]
*Phakphoom Thiravit, M.D.*[(3)]
*Thanisa Tongbai, M.D.*[(4)]
*Wiwatana Tanomkiat, M.D.*[(5)]

From [(1)]Department of Diagnostic and Therapeutic Radiology, Faculty of Medicine Ramathibodi Hospital, Mahidol University, Bangkok, Thailand.
[(2)]Department of Radiology, Faculty of Medicine, Chiangmai University, Chiangmai, Thailand.
[(3)]Department of Radiology, Faculty of Medicine Siriraj Hospital, Mahidol University, Bangkok, Thailand.
[(4)]Department of Radiology, Faculty of Medicine, Chulalongkorn University, Bangkok, Thailand.
[(5)]Department of Radiology, Faculty of Medicine, Prince of Songkla University, Songkla, Thailand.

Address correspondence to T.S. (email: ratrspoom@yahoo.com)

Received 6 April 2022 ; accepted 6 April 2022
doi:10.46475/aseanjr.v23i1.171

**Keywords:** High-resolution CT, Interstitial lung disease, Visual scoring method, Global disease extent, Fibrotic extent, Thailand.

## Introduction

Interstitial lung disease (ILD) encompasses various pulmonary parenchymal disorders [1]. Some ILDs, especially idiopathic interstitial fibrosis (IPF) and systemic sclerosis-associated ILD, can become progressive and devastating [1]. Progressive fibrosing ILD is suggested when patients having any of the following criteria have experienced disease progression in 24 months. These criteria [1] include

1. A relative decline of ≥10% in forced vital capacity (FVC);
2. A relative decline of ≥15% in diffusing capacity of the lung for carbon monoxide (*D*LCO); or
3. Worsening symptoms or a worsening radiological appearance accompanied by a ≥5–<10% relative decrease in FVC.

Early detection of ILD provides the opportunity for early therapeutic intervention, which could improve patient outcomes [1-3]. It is now generally accepted that visual abnormalities correlate with the extent of pathological involvement and the severity of physiologic impairment. Hence, determining the extent of visual abnormalities is increasingly essential for managing ILD patients, monitoring disease progression, response to therapy, and eligibility for novel antifibrotic therapies [1-3].

The ILD extent on high-resolution computed tomography (HRCT) can be quantified by visual scoring methods or quantitative CT analysis tools [4, 5]. However, due to limited resources for quantitative CT analysis, visual scoring methods for quantifying the ILD severity and the extent from HRCT remain essential.

Our previous article [6] summarizes various visual scoring methods published in the literature. Since some anatomical levels described in the previously published methods can be subject to individual interpretations [4, 6-8], we proposed a new visual scoring method for quantifying the global disease extent and the fibrotic extent on HRCT made by the consensus of the multidisciplinary working group for ILD in Thailand [9].

**Proposed visual scoring method for quantifying the ILD extent on HRCT**

The proposed visual scoring method estimates the ILD extent on HRCT in terms of the global disease extent and the fibrotic extent. Evaluation of the global disease extent helps evaluate responses (reduction or resolution of active inflammation) following immunosuppressive treatment.

The global disease extent denotes the extent of all parenchymal abnormalities related to ILD, including lung fibrosis (reticular opacities, traction bronchiolectasis, traction bronchiectasis, honeycombing, and architectural distortion) and areas with active inflammation or acute exacerbation seen as pure ground-glass opacity or consolidation [10]. The global disease extent of the ILD should not include unrelated abnormalities, e.g., active infection, concomitant emphysema secondary to cigarette smoking, pulmonary edema, mosaic perfusion, dependent atelectasis, or pseudo-ground-glass opacities caused by expiration [10-12].

Unlike the global disease extent, the fibrotic extent denotes the extent of the abnormalities showing irreversible parenchymal scarring or fibrotic changes associated with ILD. Therefore, the fibrotic extent comprises the lung areas showing reticular opacities (thickened intralobular or interlobular septa), traction bronchiolectasis, traction bronchiectasis, honeycombing, and architectural distortion [4, 10, 13, 14]. The fibrotic extent should not include any fibrotic scarring or cicatricial atelectasis due to other unrelated conditions, such as remote infection, trauma, or surgery.

Dissimilar to the previously published visual scoring methods [6], this proposed method estimates the percentage of lung involvement at the six predefined anatomical lung levels shown on HRCT. The predefined anatomical lung levels 1-5 are adopted from the previously published methods [7, 8]. Due to basal-predominant ILD, level 6 is intentionally added for a more accurate estimation of the disease extent. For a precise depiction of the predefined anatomical levels, volumetric HRCT scanning is preferred [10].

THE ASEAN JOURNAL OF RADIOLOGY
ISSN 2672-9393

The six predefined levels (Figure 1) are as follows: 1) the origin of the great vessels, immediately above the top of the aortic arch; 2) the main carina; 3) the inferior pulmonary venous confluence; 4) the halfway between levels 3 and 5; 5) immediately above the right hemidiaphragm dome; 6) 2-4 cm above the posterior costophrenic angle (basal lungs). The halfway between levels 3 and 5 can be selected based on the image number or the coronal CT images. Due to anatomical variations (e.g., diaphragmatic eventration, pulmonary vein variations), ILD severity (with severe lower-lobe volume loss), and technical issues, the levels (especially levels 4-6) chosen can be slightly different from the predefined anatomical levels and should be appropriately adjusted.

The extent of pulmonary involvement in the twelve zones (six on the right and the other six on the left) is then estimated in percentage to the nearest 5%, i.e., 0%, 5%, 10%, 15%, …,95%, 100%. A scoring tool (A and B) or arbitrary lines can be applied to aid a more precise estimation (Figure 2).

According to this method, the global disease extent and the fibrotic extent are derived from the summed percentages (extent) of these abnormalities in the six predefined levels or 12 lung zones divided by 12 (Tables 1 and 2). If level 5 is close to or similar to level 4 or 6, level 5 can be skipped. In this regard, the global disease extent and the fibrotic extent will be divided by 10 instead of 12. The global disease extent and the fibrotic extent can be reported in range, e.g., 20%-25% or 30%-35% of lung parenchyma (Tables 1 and 2).

Hence, the global disease and the fibrotic extent can be similar or different (Figure 1, Tables 1 and 2). In a patient with an inactive disease with irreversible fibrosis, the global disease and the fibrotic extent can be equal. However, the global disease extent is usually greater than the fibrotic extent in a patient having areas of pure ground-glass opacity or consolidation reflecting active interstitial inflammation or organizing pneumonia [10].

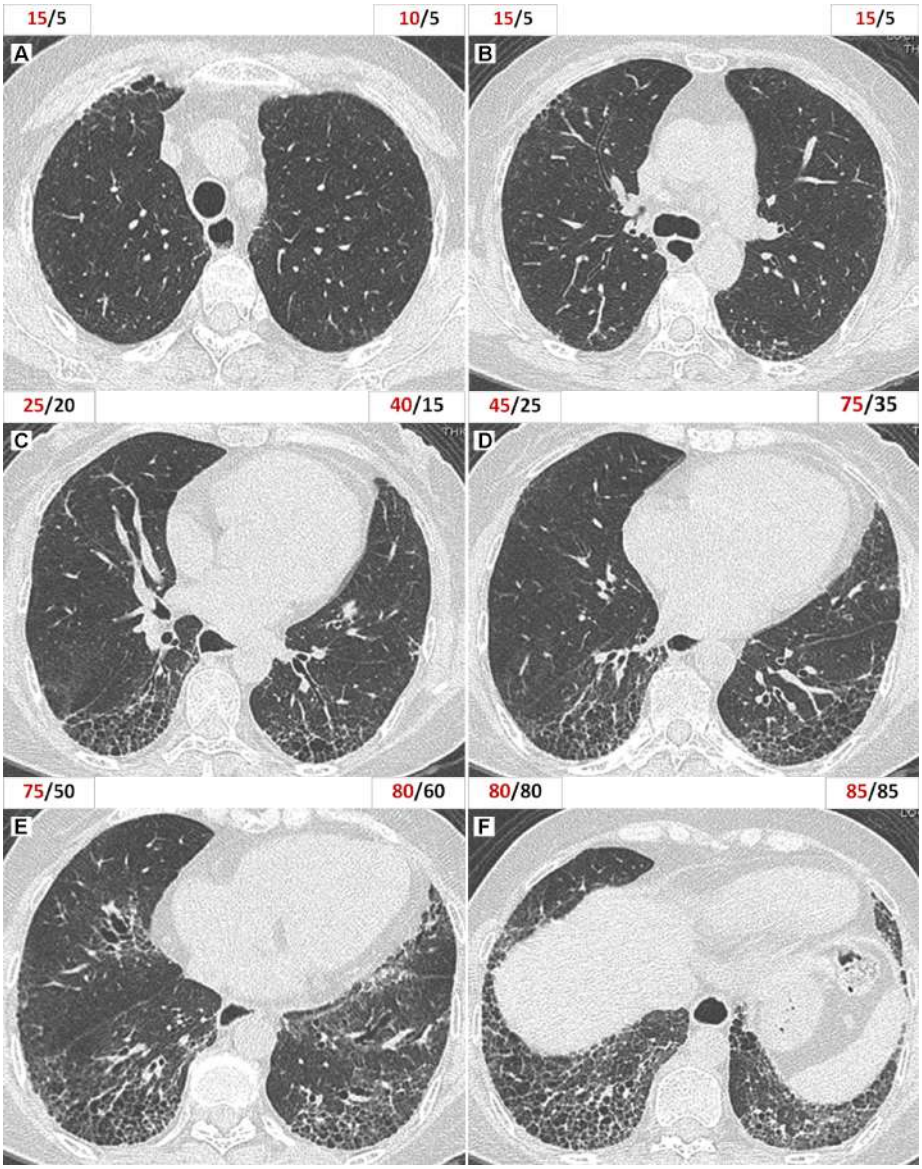


**Figure 1.** *The six predefined levels of HRCT images of a 58-year-old woman with systemic sclerosis -associated ILD, including A) level 1 (the origin of the great vessels, immediately above the top of the aortic arch), B) level 2 (the main carina), C) level 3 (the inferior pulmonary venous confluence), D) level 4 (the halfway between levels 3 and 5), E) level 5 (immediately above the right hemidiaphragm dome, and F) level 6 (2-4 cm above the posterior costophrenic angle). Each level consists of two lung zones. Pulmonary involvement in the twelve zones is estimated to be the nearest 5%. The red-colored number in each box denotes the estimated percentage of the global disease extent, whereas the black-colored number denotes the estimated percentage of the fibrotic extent.*

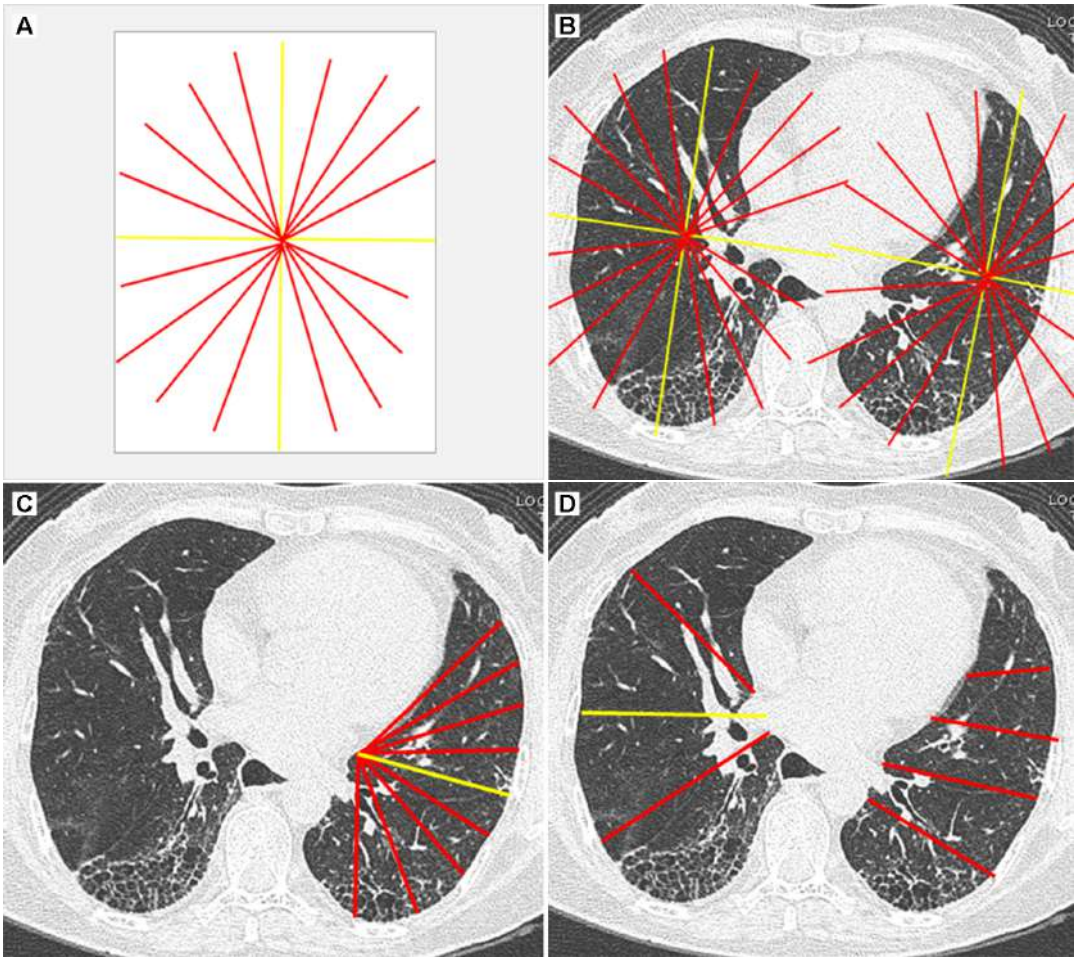


**Figure 2.** *The illustrative images showing a scoring tool (A and B) and arbitrary lines (C and D) drawn on the axial HRCT images help quantify the percentages of the global disease extent and the fibrotic extent in the right and left lungs at level 3.*

**Table 1.** *Example for calculating the global disease extent of the illustrative case in figure 1.*

| The six predefined levels | Right lung (%) | Left lung (%) | The summed extent (%) of both lungs |
|---|---|---|---|
| 1. Origin of the great vessels | 15 | 10 | 25 |
| 2. Main carina | 15 | 15 | 30 |
| 3. Inferior pulmonary venous confluence | 25 | 40 | 65 |
| 4. Halfway between level 3 and level 5 | 45 | 75 | 120 |
| 5. Immediately above the right hemidiaphragm dome | 75 | 80 | 155 |
| 6. 2-4 cm above the posterior costophrenic angles | 80 | 85 | 165 |
| Summed % of all 6 levels or 12 areas) | | | 560 |
| The global disease extent (summed % divided by 12) | | | 46.7* |

**The global disease extent can be reported as 45%-50%.*

**Table 2.** *Example for calculating the fibrotic extent of the illustrative case in figure 1.*

| The six predefined levels | Right lung (%) | Left lung (%) | The summed extent (%) of both lungs |
|---|---|---|---|
| 1. Origin of the great vessels | 5 | 5 | 10 |
| 2. Main carina | 5 | 5 | 10 |
| 3. Inferior pulmonary venous confluence | 20 | 15 | 35 |
| 4. Halfway between level 3 and level 5 | 25 | 35 | 60 |
| 5. Immediately above the right hemidiaphragm dome | 50 | 60 | 110 |
| 6. 2-4 cm above the posterior costophrenic angles | 80 | 85 | 165 |
| Summed % of all 6 levels or 12 areas) | | | 390 |
| The fibrotic extent (summed % divided by 12) | | | 32.5* |

**The fibrotic extent can be reported as 30%-35%.*

THE ASEAN JOURNAL OF RADIOLOGY
ISSN 2672-9393

It is important to note that this proposed visual scoring system roughly estimates the extent of pulmonary involvement. It does not directly determine the severity based on morphological changes, for example, coarseness of reticular interstitial abnormalities, traction bronchiolectasis, traction bronchiectasis, and honeycombing. Hence, it cannot replace standard HRCT reporting and should be interpreted along with other HRCT features. Nevertheless, this proposed visual scoring method still serves as a complementary tool for initial evaluation, monitoring progression and treatment efficacy of ILD, and facilitating communication with clinicians.

## Conclusion

The newly proposed visual scoring method for quantifying the global disease extent and the fibrotic extent on HRCT made by the consensus of the multidisciplinary working group for ILD in Thailand deems reproducible and straightforward. It is potentially helpful for managing ILD patients in monitoring disease progression, response to therapy, and eligibility for novel antifibrotic therapies.

## References

1. Cottin V, Hirani NA, Hotchkin DL, Nambiar AM, Ogura T, Otaola M, et al. Presentation, diagnosis and clinical course of the spectrum of progressive-fibrosing interstitial lung diseases. Eur Respir Rev 2018;27:180076. doi:10.1183/16000617.0076-2018.

2. Cottin V, Brown KK. Interstitial lung disease associated with systemic sclerosis (SSc-ILD). Respir Res 2019;20:13. doi: 10.1186/s12931-019-0980-7.

3. Fischer A, Patel NM, Volkmann ER. Interstitial lung disease in systemic sclerosis: focus on early detection and intervention. Open Access Rheumatol 2019;11:283-307. doi: 10.2147/oarrr.s226695.

4. Assayag D, Kaduri S, Hudson M, Hirsc A, Baron M. High resolution computed tomography scoring systems for evaluating interstitial lung disease in systemic sclerosis patients. Rheumatology 2012;S:1. doi: 10.4172/2161-1149.S1-003.

5. Chen A, Karwoski RA, Gierada DS, Bartholmai BJ, Koo CW. Quantitative CT analysis of diffuse lung disease. Radiographics 2020;40:28-43. doi:10.1148/rg.2020190099.

6. Euathrongchit J, Thiravit P, Tanomkiat W, Nitiwarangkul C, Tongbai T, Wannosopha Y, et al. Multidisciplinary working group for interstitial lung disease in Thailand: Part 2 – a concise review of published visual scoring methods for interstitial lung disease. ASEAN J Radiol In press 2022.

7. Desai SR, Veeraraghavan S, Hansell DM, Nikolakopolou A, Goh NS, Nicholson AG, et al. CT features of lung disease in patients with systemic sclerosis: comparison with idiopathic pulmonary fibrosis and nonspecific interstitial pneumonia. Radiology 2004; 232:560-7. doi: 10.1148/radiol.2322031223.

8. Goh NS, Desai SR, Veeraraghavan S, Hansell DM, Copley SJ, Maher TM, et al. Interstitial lung disease in systemic sclerosis: a simple staging system. Am J Respir Crit Care Med 2008;177:1248-54. doi: 10.1164/rccm.200706-877OC.

9. Tanomkiat W, Nitiwarangkul C, Euathrongchit J, Thiravit P, Tongbai T, Suwatanapongched T. Multidisciplinary working group for interstitial lung disease in Thailand: Part 1 – rationale in developing a guide to estimate the global disease and fibrotic extents on high-resolution computed tomography. ASEAN J Radiol [Internet]. 2021 [cited 2022 Apr1];22(3):47-60. Available from: https://www.asean-journal-radiology.org/index.php/ajr/article/view/158/106

10. Hobbs S, Chung JH, Leb J, Kaproth-Joslin K, Lynch DA. Practical imaging interpretation in patients suspected of having idiopathic pulmonary fibrosis: official recommendations from the radiology working group of the pulmonary fibrosis foundation. Radiol Cardiothorac Imaging 2021;3(1): e200279. doi: 10.1148/ryct.2021200279.

11. Oikonomou A, Prassopoulos P. Mimics in chest disease: interstitial opacities. Insights Imaging 2013;4:9-27. doi:10.1007/s13244-012-0207-7.

12. Juhl KS, Bendstrup E, Rasmussen F, Hilberg O. Emphysema mimicking interstitial lung disease: two case reports. Respir Med Case Rep 2014;15: 24-26. doi:10.1016/j.rmcr.2014.12.004.

13. Devaraj A. Imaging: how to recognise idiopathic pulmonary fibrosis. Eur Respir Rev 2014;23:215-9. doi:10.1183/09059180.00001514.

14. Jacob J, Hansell DM. HRCT of fibrosing lung disease. Respirology 2015;20: 859-72. doi:10.1111/resp.12531.

Acknowledgement of Reviewers

# Reviewer acknowledgement, 2021

*Wiwatana Tanomkiat, M.D.*

Editor-in-Chief
The ASEAN Journal of Radiology

The editor-in-chief of The ASEAN Journal of Radiology would like to thank all our reviewers who have contributed to the journal during the period from January 2021 through December 2021.

## Reviewers

| | |
|---|---|
| 1. Anchali Krisanachinda | Chulalongkorn University, Thailand |
| 2. Arthur Edward Brown | Mahidol University, Thailand |
| 3. Juntima Euathrongchit | Chiang Mai University, Thailand |
| 4. Kamonwon Cattapan | Prince of Songkla University, Thailand |
| 5. Keerati Hongsakul | Prince of Songkla University, Thailand |
| 6. Linda Brown | Mahidol University, Thailand |
| 7. Monravee Tumkosit | Chulalongkorn University, Thailand |
| 8. Nantaka Kiranantawat | Prince of Songkla University, Thailand |
| 9. Napapong Pongnapang | Mahidol University, Thailand |
| 10. Nitra Piyavisetpat | MedPark Hospital, Thailand |
| 11. Panaya Tumsatan | Khon Kaen University, Thailand |
| 12. Phakphoom Thiravit | Mahidol University, Thailand |
| 13. Rathachai Kaewlai | Mahidol University, Thailand |
| 14. Ruedeekorn Suwannanon | Prince of Songkla University, Thailand |
| 15. Saowapa Angsupanich | Prince of Songkla University, Thailand |
| 16. Sarayut Geater | Prince of Songkla University, Thailand |
| 17. Siriporn Leelakiatpaiboon | Prince of Songkla University, Thailand |
| 18. Supawitoo Sookpeng | Naresuan University, Thailand |
| 19. Suwimon Wonglaksanapimon | Mahidol University, Thailand |
| 20. Thanisa Tongbai | Chulalongkorn University, Thailand |
| 21. Warawut Sukkasem | Mahidol University, Thailand |
| 22. Woranut Iampa | Mahidol University, Thailand |
| 23. Yutthaphan Wannasopha | Chiangmai University, Thailand |

ASEAN

**This journal provide 4 areas of editorial services: language editing, statistical editing, content editing, and complete reference-citation check in 8 steps:**

| Step | Services to authors | Services providers |
|---|---|---|
| I | Manuscript submitted | Editor |
| II | Language editing/ A reference-citation check | Language consultant/Bibliographer |
| III | First revision to ensure that all information remains correct after language editing | Editor |
| IV | Statistical editing | Statistical consultant |
| V | Content editing* | Two reviewers |
| VI | Second revision | Editor |
| VII | Manuscript accepted/ rejected | Editor/Editorial board |
| VIII | Manuscript published | Editorial office |

*Content editing follows a double-blind reviewing procedure

JOURNAL OF RADIOLOGY